Table 4. Patient characteristics

	Patients treated by TAE (n = 20)	Patients treated by TAE with DC (n = 13)	p-value[1]
Age (years)[2]	66.6 ± 7.8	65.7 ± 10.0	NS
Sex (M/F)	14/6	11/2	NS
HLA (A23 or 24/others)	16/4	9/4	NS
ALT (IU/l)	51.0 ± 47.4	86.9 ± 62.8	NS
Total bilirubin (g/dl)	1.3 ± 0.9	1.5 ± 0.9	NS
Albumin (g/dl)	3.7 ± 0.7	3.2 ± 0.6	NS
AFP level (ng/ml)	322.7 ± 793.0	239.8 ± 418.2	NS
Diff. degrees of HCC (well/moderate or poor/ND[1])	2/6/12	4/4/5	NS
Tumor size (small/large[3])	4/16	1/12	NS
Tumor multiplicity (multiple/solitary)	18/2	12/1	NS
TNM stage (I, II/III, IV)	19/1	11/2	NS
Histology of nontumor liver (LC/chronic hepatitis)	15/5	10/3	NS
Liver function (Child A/B or C)	14/6	3/10	0.02
Etiology (HCV/HBV/others)	12/2/6	13/0/0	NS

[1]Abbreviations: NS, no statistical significance; ND, not determined. [2]Data are expressed as the mean ± SD. [3]Small: ≤2 cm, large: >2 cm.

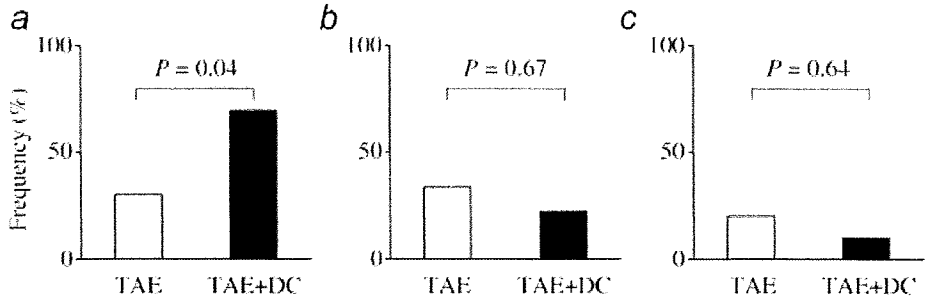

Figure 2. Frequency of the patients who showed enhancement of T-cell responses after treatment. The prevalence of antigen-specific T cells was determined by IFN-γ ELISPOT analysis using alpha-fetoprotein (AFP) and AFP-derived peptides (*a*), CMV pp65-derived peptide (*b*) or tetanus toxoid protein (*c*) in 20 and 13 patients with HCC who received TAE and TAE with DC infusion, respectively.

in 4 and 6 patients who did and did not show increasing AFP-specific T-cell responses, respectively.

Kinetics of AFP-specific T-cell responses before and after TAE

Next, we examined the kinetics of AFP-specific T cells in 8 patients who showed increasing frequency of IFN-γ-producing T cells against AFP or AFP-derived peptides after TAE. The frequency was examined by ELISPOT assay before and 2–4 weeks and 3 months after TAE. Thirteen kinds of AFP-specific T cells showed increasing frequency 2–4 weeks after TAE (Fig. 4); however, the increase was transient and most cell types decreased 3 months after TAE. Three patients showed more than 10 specific spots for AFP or AFP-derived peptides 3 months after TAE (Patients 6, 11 and 30). In analysis of the correlation between the maintenance of AFP-specific T-cell responses and HCC recurrence, 1 patient (Patient 6) had HCC recurrence after 6 months and 1 patient (Patient 30) did not show recurrence. Another patient (Patient 11) did not receive curative ablation and was not analyzed. There was no difference in the kinetics of AFP-specific T cells between patients who received TAE with and without DC infusion.

Discussion

In a previous study, we made a preliminary report that immune responses specific for tumor antigens were enhanced after HCC treatments.[7,10] Similarly, as in our previous or other group's results,[8] we observed enhancement of AFP-specific immune responses in 6 of 20 patients with TAE alone in this study. The enhancement of tumor antigen-specific immune responses was also observed in the cases using MRP3- or hTERT-derived peptides.

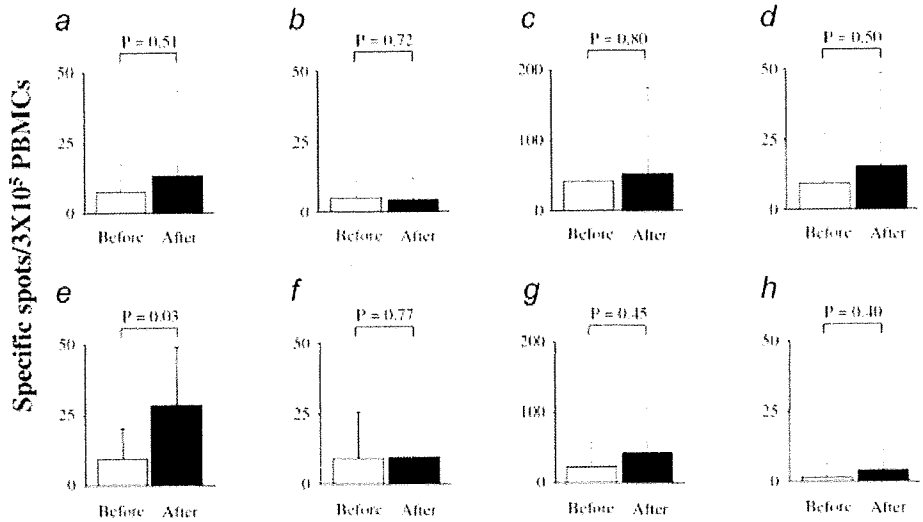

Figure 3. Comparison of direct *ex vivo* analysis (IFN-γ ELISPOT assay) before and after treatment of HCC. The assay was performed using PBMCs of patients who received TAE for AFP-derived peptides (*a*), AFP (*b*), CMV pp65-derived peptide (*c*) or tetanus toxoid protein (*d*). The same assay was performed using PBMCs of patients who received TAE with DC infusion for AFP-derived peptides (*e*), AFP (*f*), CMV pp65-derived peptide (*g*) or tetanus toxoid protein (*h*). AFP and CMV pp65-derived peptides were tested in only HLA-A24 or A23 positive patients. Data are expressed as the mean + SD of specific spots.

Table 5. Characteristics of the patients with HLA-A24 or A23

	Patients treated by TAE (n = 16)	Patients treated by TAE with DC (n = 9)	p-value[1]
Age (years)[2]	65.7 ± 7.8	67.8 ± 10.8	NS
Sex (M/F)	10/6	7/2	NS
ALT (IU/l)	55.9 ± 51.9	75.4 ± 53.0	NS
Total bilirubin (g/dl)	1.4 ± 0.8	1.4 ± 1.1	NS
Albumin (g/dl)	3.6 ± 0.7	3.1 ± 0.6	NS
AFP level (ng/ml)	392.1 ± 877.8	337.2 ± 477.1	NS
Diff. degree of HCC (well/moderate or poor/ND[1])	2/5/9	3/3/3	NS
Tumor size (small/large[3])	3/13	0/9	NS
Tumor multiplicity (multiple/solitary)	15/1	8/1	NS
TNM stage (I, II/III, IV)	15/1	7/2	NS
Histology of nontumor liver (LC/chronic hepatitis)	13/3	8/1	NS
Liver function (Child A/B or C)	10/6	0/9	0.003
Etiology (HCV/HBV/others)	11/1/4	9/0/0	NS

[1]Abbreviations: NS, no statistical significance; ND, not determined. [2]Data are expressed as the mean ± SD. [3]Small: ≤2 cm, large: >2 cm.

The precise mechanism of this phenomenon is still unknown; however, in recent studies, several treatments to destroy tumor cells by necrosis and/or apoptosis have induced antitumor immune responses in animal models[14,44] and even in humans.[6–10] In the study of *in situ* tumor ablation, it is reported that tumor ablation creates a tumor antigen source for the induction of antitumor immunity.[9,44] In another study regarding photodynamic therapy (PDT),[45] it is reported that acute inflammation, expression of heat-shock proteins and providing tumor antigens to DCs caused by PDT induce tumor-specific immune responses.

Based on these results, we hypothesize that DC infusion with TAE can induce antitumor immune responses more effectively than TAE alone. According to DC research in recent years, successful enhancement of the antitumor immune response has been reported by intratumoral

Table 6. Enhancement of AFP-specific T cell response and treatment outcome

	Enhancement of AFP-specific T cell response	Recurrence, 3 months	Recurrence, 6 months
Patient 1	−	N	U
Patient 2	−	N	M
Patient 4	+	M	ND
Patient 5	−	N	M
Patient 6	+	N	U
Patient 9	−	N	M
Patient 10	−	N	N
Patient 13	−	N	N
Patient 14	−	N	N
Patient 16	−	N	M
Patient 19	−	N	U
Patient 24	+	U	ND
Patient 25	+	M	ND
Patient 26	+	N	N
Patient 30	+	N	N
Patient 31	+	N	N
Patient 33	−	N	N

Abbreviations: N, no recurrence; U, uninodular recurrence; M, multinodular recurrence; ND, not determined.

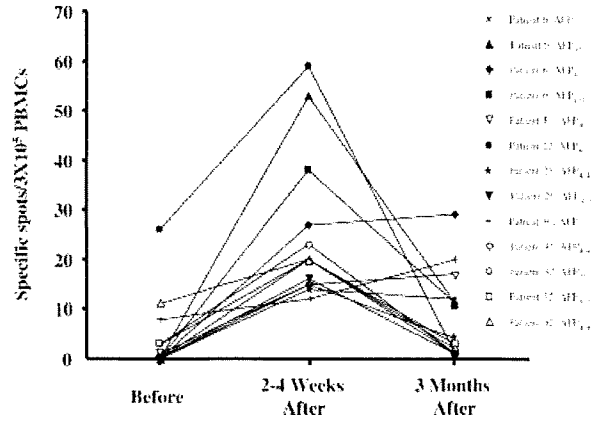

Figure 4. Kinetics of AFP-specific T-cell responses determined by IFN-γ ELISPOT assay before and after TAE. PBMCs were obtained before and 2–4 weeks and 3 months after TAE. Each graph indicates the kinetics of T cells specific for each antigen in each patient. Some patients received additional treatments as indicated in Tables 1 and 3 for a curative treatment after the measurement of T-cell responses at 2–4 weeks after TAE.

administration of DC in combination with tumor ablation.[46,47] Furthermore, immunotherapies using DC have been performed in patients with HCC and their antitumor effects are reported.[48–50] These results support our hypothesis and therefore, in the next step, we examined the immunological effects of DC infusion with TAE.

The comparison of frequency in patients who showed enhancement of AFP-specific immune responses revealed more frequency in patients with DC infusion than in those with TAE alone. On the other hand, there were no differences in the 2 groups in the comparison of frequency for patients who showed enhancement of CMV or TT-specific immune responses. These results suggest that DC infusion with TAE affects tumor-specific immune responses and that the effects are limited to the tumor area.

Some patients with TAE alone showed disappearance of AFP- or control antigen-specific T cells. Although the mechanism of this phenomenon is unknown, anticancer drugs used in TAE might suppress the immune responses, because most of the patients showed decreasing the number of lymphocytes after TAE. These results suggest that TAE alone might give a chance to enhance tumor-specific T-cell responses in only some patients. Further analysis using many more patients with TAE is necessary to make clear the differences in the patients with and without enhancement of T-cell responses. In contrast, disappearance of AFP- or control antigen-specific T cells was not observed in the patients with DC infusion, suggesting strong immunostimulating effect of this treatment.

In analysis of the association between the enhancement of AFP-specific T cells and clinical responses, no correlation could be shown, suggesting that enhancement of T-cell response associated with TAE or TAE with DC infusion may not have protective effect against HCC recurrence. To clarify the mechanism in more detail, we examined the kinetics of AFP-specific T-cell response. Increased frequency of AFP-specific T cells was transient and fell in 4 of 8 patients 3 months after treatment (Fig. 4). Similar to our results, Ayaru *et al.* also reported that the frequency of AFP-specific $CD4^+$ T cells fell in all patients by 1–3 months after TAE.[8] In addition, our results suggest that DC infusion with TAE is not effective to maintain the increased frequency of AFP-specific T cells.

Recent genome profiling studies of HCC show that HCC is a very heterogenous tumor.[51] Furthermore, HCC has multicentric carcinogenesis and develops at different time points. These characters of HCC may also be another reason for no correlation between the enhancement of AFP-specific T cells and clinical responses. The identification of many more tumor antigens and their T-cell epitopes is necessary for more precise analysis of the relationship between antitumor immune response and clinical response, and for immunotherapy.

In the recent study, it is reported that $CD8^+$ T-cell response to AFP is multispecific and AFP-specific IFN-γ-producing $CD8^+$ T cells are directed against different epitopes spreading over the entire AFP sequence with no single

immuno-dominant CD8$^+$ T-cell epitope.[52] Therefore, there is a limitation to our study, because the number of immunogenic AFP-derived peptides applicable in this study is small. However, the results of the present study suggest that TAE with DC infusion enhances the tumor-specific immune responses. Although these modified immune responses may not be sufficient to prevent HCC recurrence because the enhanced immune responses are transient and attenuate within 3 months, these results may contribute to the development of novel immunotherapeutic approach for HCC.

Acknowledgements

The authors thank Ms. Maki Kawamura and Ms. Kazumi Fushimi for technical assistance and for their invaluable help with sample collection.

References

1. Curley SA, Izzo F, Ellis LM, Nicolas Vauthey J, Vallone P. Radiofrequency ablation of hepatocellular cancer in 110 patients with cirrhosis. *Ann Surg* 2000;232: 381–91.
2. Mazzaferro V, Regalia E, Doci R, Andreola S, Pulvirenti A, Bozzetti F, Montalto F, Ammatuna M, Morabito A, Gennari L. Liver transplantation for the treatment of small hepatocellular carcinomas in patients with cirrhosis. *N Engl J Med* 1996;334: 693–9.
3. Urabe T, Kaneko S, Matsushita E, Unoura M, Kobayashi K. Clinical pilot study of intrahepatic arterial chemotherapy with methotrexate, 5-fluorouracil, cisplatin and subcutaneous interferon-alpha-2b for patients with locally advanced hepatocellular carcinoma. *Oncology* 1998; 55:39–47.
4. Ishizaki Y, Kawasaki S. The evolution of liver transplantation for hepatocellular carcinoma (past, present, and future). *J Gastroenterol* 2008;43:18–26.
5. Okuwaki Y, Nakazawa T, Shibuya A, Ono K, Hidaka H, Watanabe M, Kokubu S, Saigenji K. Intrahepatic distant recurrence after radiofrequency ablation for a single small hepatocellular carcinoma: risk factors and patterns. *J Gastroenterol* 2008;43:71–8.
6. Abdel-Hady ES, Martin-Hirsch P, Duggan-Keen M, Stern PL, Moore JV, Corbitt G, Kitchener HC, Hampson IN. Immunological and viral factors associated with the response of vulval intraepithelial neoplasia to photodynamic therapy. *Cancer Res* 2001;61:192–6.
7. Nakamoto Y, Mizukoshi E, Tsuji H, Sakai Y, Kitahara M, Arai K, Yamashita T, Yokoyama K, Mukaida N, Matsushima K, Matsui O, Kaneko S. Combined therapy of transcatheter hepatic arterial embolization with intratumoral dendritic cell infusion for hepatocellular carcinoma: clinical safety. *Clin Exp Immunol* 2007;147: 296–305.
8. Ayaru L, Pereira SP, Alisa A, Pathan AA, Williams R, Davidson B, Burroughs AK, Meyer T, Behboudi S. Unmasking of alpha-fetoprotein-specific CD4(+) T cell responses in hepatocellular carcinoma patients undergoing embolization. *J Immunol* 2007;178:1914–22.
9. Zerbini A, Pilli M, Penna A, Pelosi G, Schianchi C, Molinari A, Schivazappa S, Zibera C, Fagnoni FF, Ferrari C, Missale G. Radiofrequency thermal ablation of hepatocellular carcinoma liver nodules can activate and enhance tumor-specific T-cell responses. *Cancer Res* 2006;66:1139–46.
10. Mizukoshi E, Nakamoto Y, Tsuji H, Yamashita T, Kaneko S. Identification of alpha-fetoprotein-derived peptides recognized by cytotoxic T lymphocytes in HLA-A24+ patients with hepatocellular carcinoma. *Int J Cancer* 2006;118: 1194–204.
11. Gollnick SO, Evans SS, Baumann H, Owczarczak B, Maier P, Vaughan L, Wang WC, Unger E, Henderson BW. Role of cytokines in photodynamic therapy-induced local and systemic inflammation. *Br J Cancer* 2003;88:1772–9.
12. Gollnick SO, Owczarczak B, Maier P. Photodynamic therapy and anti-tumor immunity. *Lasers Surg Med* 2006;38: 509–15.
13. Yamamoto N, Homma S, Sery TW, Donoso LA, Hoober JK. Photodynamic immunopotentiation: in vitro activation of macrophages by treatment of mouse peritoneal cells with haematoporphyrin derivative and light. *Eur J Cancer* 1991;27: 467–71.
14. den Brok MH, Sutmuller RP, van der Voort R, Bennink EJ, Figdor CG, Ruers TJ, Adema GJ. In situ tumor ablation creates an antigen source for the generation of antitumor immunity. *Cancer Res* 2004;64: 4024–9.
15. Kotera Y, Shimizu K, Mule JJ. Comparative analysis of necrotic and apoptotic tumor cells as a source of antigen(s) in dendritic cell-based immunization. *Cancer Res* 2001; 61:8105–9.
16. Sauter B, Albert ML, Francisco L, Larsson M, Somersan S, Bhardwaj N. Consequences of cell death: exposure to necrotic tumor cells, but not primary tissue cells or apoptotic cells, induces the maturation of immunostimulatory dendritic cells. *J Exp Med* 2000;191:423–34.
17. Korbelik M, Sun J, Cecic I. Photodynamic therapy-induced cell surface expression and release of heat shock proteins: relevance for tumor response. *Cancer Res* 2005;65: 1018–26.
18. Takayasu K, Arii S, Ikai I, Omata M, Okita K, Ichida T, Matsuyama Y, Nakanuma Y, Kojiro M, Makuuchi M, Yamaoka Y. Prospective cohort study of transarterial chemoembolization for unresectable hepatocellular carcinoma in 8510 patients. *Gastroenterology* 2006;131:461–9.
19. Matsui O, Kadoya M, Yoshikawa J, Gabata T, Arai K, Demachi H, Miyayama S, Takashima T, Unoura M, Kogayashi K. Small hepatocellular carcinoma: treatment with subsegmental transcatheter arterial embolization. *Radiology* 1993;188:79–83.
20. Yamada R, Kishi K, Sonomura T, Tsuda M, Nomura S, Satoh M. Transcatheter arterial embolization in unresectable hepatocellular carcinoma. *Cardiovasc Intervent Radiol* 1990;13:135–9.
21. Pelletier G, Roche A, Ink O, Anciaux ML, Derhy S, Rougier P, Lenoir C, Attali P, Etienne JP. A randomized trial of hepatic arterial chemoembolization in patients with unresectable hepatocellular carcinoma. *J Hepatol* 1990;11:181–4.
22. Groupe d'Etude et de Traitement du Carcinome Hepatocellulaire. A comparison of lipiodol chemoembolization and conservative treatment for unresectable hepatocellular carcinoma. *N Engl J Med* 1995;332:1256–61.
23. Bruix J, Llovet JM, Castells A, Montana X, Bru C, Ayuso MC, Vilana R, Rodes J. Transarterial embolization versus symptomatic treatment in patients with advanced hepatocellular carcinoma: results of a randomized, controlled trial in a single institution. *Hepatology* 1998;27:1578–83.
24. Llovet JM, Real MI, Montana X, Planas R, Coll S, Aponte J, Ayuso C, Sala M, Muchart J, Sola R, Rodes J, Bruix J. Arterial embolisation or chemoembolisation versus symptomatic treatment in patients with unresectable hepatocellular carcinoma: a randomised controlled trial. *Lancet* 2002;359:1734–9.
25. Lo CM, Ngan H, Tso WK, Liu CL, Lam CM, Poon RT, Fan ST, Wong J. Randomized controlled trial of transarterial lipiodol chemoembolization for unresectable hepatocellular carcinoma. *Hepatology* 2002;35:1164–71.
26. Hsu HC, Wei TC, Tsang YM, Wu MZ, Lin YH, Chuang SM. Histologic assessment of resected hepatocellular carcinoma after

transcatheter hepatic arterial embolization. *Cancer* 1986;57:1184–91.
27. Kenji J, Hyodo I, Tanimizu M, Tanada M, Nishikawa Y, Hosokawa Y, Mandai K, Moriwaki S. Total necrosis of hepatocellular carcinoma with a combination therapy of arterial infusion of chemotherapeutic lipiodol and transcatheter arterial embolization: report of 14 cases. *Semin Oncol* 1997;24: S6-71–S6-80.
28. Kobayashi N, Ishii M, Ueno Y, Kisara N, Chida N, Iwasaki T, Toyota T. Co-expression of Bcl-2 protein and vascular endothelial growth factor in hepatocellular carcinomas treated by chemoembolization. *Liver* 1999;19:25–31.
29. Xiao EH, Li JQ, Huang JF. Effects of p53 on apoptosis and proliferation of hepatocellular carcinoma cells treated with transcatheter arterial chemoembolization. *World J Gastroenterol* 2004;10:190–4.
30. Kanai M, Kohda H, Sekiya C, Namiki M. Effects on interleukin 1 alpha and beta production of peripheral blood mononuclear cells from patients with hepatocellular carcinoma after transcatheter arterial embolization. *Gastroenterol Jpn* 1990;25:662.
31. Yamazaki H, Nishimoto N, Oi H, Matsushita M, Ogata A, Shima Y, Inoue T, Tang JT, Yoshizaki K, Kishimoto T, Inoue T. Serum interleukin 6 as a predicator of the therapeutic effect and adverse reactions after transcatheter arterial embolization. *Cytokine* 1995;7:191–5.
32. Itoh Y, Okanoue T, Ohnishi N, Nishioji K, Sakamoto S, Nagao Y, Nakamura H, Kirishima T, Kashima K. Hepatic damage induced by transcatheter arterial chemoembolization elevates serum concentrations of macrophage-colony stimulating factor. *Liver* 1999;19:97–103.
33. Araki T, Itai Y, Furui S, Tasaka A. Dynamic CT densitometry of hepatic tumors. *AJR Am J Roentgenol* 1980;135: 1037–43.
34. Sobin LH, Wittekind C. TNM classification of malignant tumors, 6th edn. New York: Wiley-Liss, 2002. 81.
35. Terayama N, Miyayama S, Tatsu H, Yamamoto T, Toya D, Tanaka N, Mitsui T, Miura S, Fujisawa M, Kifune K, Matsui O, Takashima T. Subsegmental transcatheter arterial embolization for hepatocellular carcinoma in the caudate lobe. *J Vasc Interv Radiol* 1998;9:501–8.
36. Okamoto H, Shin J, Mion S, Koshimura S, Shimizu R. Studies on the anticancer and streptolysin S-forming abilities of hemolytic streptococci. *Jpn J Microbiol* 1967;11: 323–36.
37. Nakahara S, Tsunoda T, Baba T, Asabe S, Tahara H. Dendritic cells stimulated with a bacterial product, OK-432, efficiently induce cytotoxic T lymphocytes specific to tumor rejection peptide. *Cancer Res* 2003; 63:4112–8.
38. Japan LCSGo. Classification of primary liver cancer. English edn. 2. Tokyo: Kanehara, 1997.
39. Desmet VJ, Gerber M, Hoofnagle JH, Manns M, Scheuer PJ. Classification of chronic hepatitis: diagnosis, grading and staging. *Hepatology* 1994;19:1513–20.
40. Mizukoshi E, Nakamoto Y, Marukawa Y, Arai K, Yamashita T, Tsuji H, Kuzushima K, Takiguchi M, Kaneko S. Cytotoxic T cell responses to human telomerase reverse transcriptase in patients with hepatocellular carcinoma. *Hepatology* 2006;43:1284–94.
41. Mizukoshi E, Honda M, Arai K, Yamashita T, Nakamoto Y, Kaneko S. Expression of multidrug resistance-associated protein 3 and cytotoxic T cell responses in patients with hepatocellular carcinoma. *J Hepatol* 2008;49:946–54.
42. Ikeda-Moore Y, Tomiyama H, Miwa K, Oka S, Iwamoto A, Kaneko Y, Takiguchi M. Identification and characterization of multiple HLA-A24-restricted HIV-1 CTL epitopes: strong epitopes are derived from V regions of HIV-1. *J Immunol* 1997;159: 6242–52.
43. Kuzushima K, Hayashi N, Kimura H, Tsurumi T. Efficient identification of HLA-A*2402-restricted cytomegalovirus-specific CD8(+) T-cell epitopes by a computer algorithm and an enzyme-linked immunospot assay. *Blood* 2001;98:1872–81.
44. Wissniowski TT, Hansler J, Neureiter D, Frieser M, Schaber S, Esslinger B, Voll R, Strobel D, Hahn EG, Schuppan D. Activation of tumor-specific T lymphocytes by radio-frequency ablation of the VX2 hepatoma in rabbits. *Cancer Res* 2003;63: 6496–500.
45. Korbelik M, Krosl G, Krosl J, Dougherty GJ. The role of host lymphoid populations in the response of mouse EMT6 tumor to photodynamic therapy. *Cancer Res* 1996;56: 5647–52.
46. Udagawa M, Kudo-Saito C, Hasegawa G, Yano K, Yamamoto A, Yaguchi M, Toda M, Azuma I, Iwai T, Kawakami Y. Enhancement of immunologic tumor regression by intratumoral administration of dendritic cells in combination with cryoablative tumor pretreatment and Bacillus Calmette-Guerin cell wall skeleton stimulation. *Clin Cancer Res* 2006;12: 7465–75.
47. Machlenkin A, Goldberger O, Tirosh B, Paz A, Volovitz I, Bar-Haim E, Lee SH, Vadai E, Tzehoval E, Eisenbach L. Combined dendritic cell cryotherapy of tumor induces systemic antimetastatic immunity. *Clin Cancer Res* 2005;11: 4955–61.
48. Ladhams A, Schmidt C, Sing G, Butterworth L, Fielding G, Tesar P, Strong R, Leggett B, Powell L, Maddern G, Ellem K, Cooksley G. Treatment of non-resectable hepatocellular carcinoma with autologous tumor-pulsed dendritic cells. *J Gastroenterol Hepatol* 2002;17: 889–96.
49. Iwashita Y, Tahara K, Goto S, Sasaki A, Kai S, Seike M, Chen CL, Kawano K, Kitano S. A phase I study of autologous dendritic cell-based immunotherapy for patients with unresectable primary liver cancer. *Cancer Immunol Immunother* 2003; 52:155–61.
50. Lee WC, Wang HC, Hung CF, Huang PF, Lia CR, Chen MF. Vaccination of advanced hepatocellular carcinoma patients with tumor lysate-pulsed dendritic cells: a clinical trial. *J Immunother* 2005;28: 496–504.
51. Lee JS, Thorgeirsson SS. Genome-scale profiling of gene expression in hepatocellular carcinoma: classification, survival prediction, and identification of therapeutic targets. *Gastroenterology* 2004; 127:S51–5.
52. Thimme R, Neagu M, Boettler T, Neumann-Haefelin C, Kersting N, Geissler M, Makowiec F, Obermaier R, Hopt UT, Blum HE, Spangenberg HC. Comprehensive analysis of the alpha-fetoprotein-specific CD8+ T cell responses in patients with hepatocellular carcinoma. *Hepatology* 2008;48:1821–33.

Crucial Contribution of Thymic Sirpα^+ Conventional Dendritic Cells to Central Tolerance against Blood-Borne Antigens in a CCR2-Dependent Manner

Tomohisa Baba,* Yasunari Nakamoto,† and Naofumi Mukaida[1]*

Thymic dendritic cells (DCs) as well as thymic epithelial cells are presumed to be major sentinels in central tolerance by inducing the apoptosis of autoreactive T progenitor cells. The thymic DC population is composed of heterogeneous subsets including CD11c$^+$B220$^+$ plasmacytoid DCs, CD11c$^+$B220$^-$CD8α^+ signal regulatory protein α (Sirpα)$^-$ and CD11c$^+$B220$^-$CD8α^-Sirpα^+ conventional DCs (cDCs). However, the distinctive role of each DC subset remains undefined. We show herein that Sirpα^+ cDCs, a minor subpopulation, was disseminated in the thymic cortical area with some of them uniquely localized inside perivascular regions and nearby small vessels in the thymus. The Sirpα^+ but not Sirpα^- cDC subset can selectively capture blood-circulating Ags. Moreover, in CCR2-deficient mice, the thymic Sirpα^+ cDC subset, but not other thymic cell components, was moderately decreased especially in the perivascular regions. Concomitantly, these mice exhibited a modest impairment in intrathymic negative selection against blood-borne Ags, with the reduced capacity to uptake blood-borne Ags. Given their intrathymic cortical localization, CD11c$^+$B220$^-$CD8α^-Sirpα^+ cDCs can have a unique role in the development of central tolerance against circulating peripheral Ags, at least partially in a CCR2-dependent manner. *The Journal of Immunology,* **2009, 183: 3053–3063.**

The thymus is vital for development of T cells. T progenitor cells in the thymus are subjected to positive and negative selection, and survivors become self-MHC-restricted and self-tolerant mature naive T cells. Negative selection induces clonal deletion of potentially pathogenic autoreactive T cells and consequently decreases the risk of the development of autoimmune disorders (1). Thus, negative selection has a major role in central tolerance. Medullary thymic epithelial cells (mTECs)[2] are major inducers of negative selection. mTECs express the *autoimmune regulator (AIRE)* gene, which induces the ectopic expression of a milieu of peripheral tissue-specific Ags in the thymus resulting in the clonal deletion of autoreactive T progenitors with specificity for these Ags (2–4). Another type of thymic APCs, in particularly dendritic cells (DCs), have also been shown to contribute to negative selection (5–7). However, the detailed molecular and cellular mechanisms by which thymic DCs mediate negative selection remain largely unknown.

Thymic DCs are heterogeneous, similar to DCs in peripheral lymphoid organs such as lymph nodes and spleen. In humans and mice, thymic DCs are classified into two distinct subsets, CD11c$^+$B220$^+$ plasmacytoid DCs (pDCs) and CD11c$^+$B220$^-$ conventional DCs (cDCs). cDCs are further divided into CD11c$^+$CD11b$^-$CD8α^+Sirpα^- and CD11c$^+$CD11b$^+$CD8α^-Sirpα^+ subsets (8, 9). CD8α^+Sirpα^- cDCs, the most abundant subset among these three thymic DC subsets, are clustered in the medulla (10, 11). These CD8α^+Sirpα^- cDCs also express AIRE and can present endogenous self-Ags. In addition, they can cross-present tissue-specific Ags derived from the mTECs for negative selection (12, 13). In contrast, the intrathymic location and functions of another minor cDC, CD11c$^+$CD11b$^+$CD8α^-Sirpα^+, subset remain unclear, although this subset is presumed to migrate from the bloodstream (8). Proietto et al. (14) demonstrated that Sirpα^+ cDCs can induce thymocytes to efficiently differentiate into regulatory T cells in vitro. However, the roles of Sirpα^+ cDCs in central tolerance and regulatory T cell generation in vivo and the nature of the target autoantigens of central tolerance remain elusive.

Chemokines and their receptors have essential roles in controlling the homeostatic homing of immune cells including DCs and T cells (15–17). We examined the composition of thymic DC subsets in mice deficient in CCR1, CCR2, CCR5, or CX3CR1, the chemokine receptors which are expressed by DCs (18, 19). We observed that Sirpα^+ cDCs, but not Sirpα^- cDCs or pDCs, were selectively decreased in the thymus of CCR2-deficient mice, but not in the other chemokine receptor gene-deficient mice. Interestingly, CCR2-deficient mice exhibited a modest impairment in intrathymic negative selection against i.v. injected Ags. Concomitantly, CCR2 deficiency allowed releasing more autoreactive T cells against serum Ags into periphery. These Sirpα^+ cDCs migrated from bone marrow to thymus by the way of the peripheral blood and showed a unique intrathymic localization confined to perivascular and cortical areas. Moreover, Sirpα^+ cDCs had a greater capacity to uptake blood-borne Ags than Sirpα^- cDCs, along with their unique intrathymic localization. Thus, our present study suggests that thymic Sirpα^+ cDCs may function as a specialized APC for the development of central tolerance to blood-borne Ags.

*Division of Molecular Bioregulation, Cancer Research Institute and †Department of Disease Control and Homeostasis, Graduate School of Medical Science, Kanazawa University, Kanazawa, Ishikawa, Japan

Received for publication February 13, 2009. Accepted for publication June 8, 2009.

The costs of publication of this article were defrayed in part by the payment of page charges. This article must therefore be hereby marked *advertisement* in accordance with 18 U.S.C. Section 1734 solely to indicate this fact.

[1] Address correspondence and reprint requests to Dr. Naofumi Mukaida, Division of Molecular Bioregulation, Cancer Research Institute, Kanazawa University, 13-1 Takara-machi, Kanazawa 920-0934, Japan. E-mail address: naofumim@kenroku.kanazawa-u.ac.jp

[2] Abbreviations used in this paper: mTEC, medullary thymic epithelial cell; DC, dendritic cell; Sirpα, signal regulatory protein α; pDC, plasmacytoid DC; cDC, conventional DC; WT, wild type; Col IV, type IV collagen; FCM, flow cytometry; CMFDA, 5-chloromethylfluorescien diacetate; Cyt D, cytochalasin D; FSC, forward scatter; SSC, side scatter; DP, double positive.

www.jimmunol.org/cgi/doi/10.4049/jimmunol.0900438

Materials and Methods

Mice

Specific pathogen-free 6- to 7-wk-old male BALB/c mice were purchased from Charles River Japan and designated as wild-type (WT) mice. CCR1$^{-/-}$ and CX3CR1$^{-/-}$ mice were provided by Dr. P. M. Murphy (National Institute of Allergy and Infectious Diseases, National Institutes of Health, Bethesda, MD) (20, 21). CCR2$^{-/-}$ (22) and CCR5$^{-/-}$ mice (23) were provided by Dr. W. Kuziel (University of Texas San Antonio, San Antonio, TX) and Dr. Kouji Matsushima (University of Tokyo, Tokyo, Japan), respectively. All chemokine receptor-deficient mice were backcrossed to BALB/c mice for 8–10 generations. DO11.10 mice expressing a transgenic TCR that recognizes the $OVA_{323-339}$ peptide in the context of I-A^d were maintained as heterozygotes. DO11.10 mice were backcrossed to CCR2$^{-/-}$ mice to generate DO11.10/CCR2$^{-/-}$ mice. Genotyping for the *CCR2* gene was done by direct PCR from whole blood samples using an Ampdirect Plus kit (Shimadzu) and the specific primers (sense, 5′-CACGAAGTATCCAAGAGCTTG-3′ and antisense, 5′-CCCAAGTGAC TACACTTGTTA-3′). The mouse experiments were performed under specific pathogen-free conditions in accordance with the Guidelines for the Care and Use of Laboratory Animals of Kanazawa University.

Antibodies

Rat anti-mouse mAbs used were anti-CD3ε (145-2C11; Miltenyi Biotec), anti-CD4 (RM4-5; BD Pharmingen), anti-CD8 (53-6.7; BD Pharmingen), anti-CD25 (PC61; BD Pharmingen), anti-CD45R/B220 (RA3-6B2; BD Pharmingen), anti-CD172a/Sirpα (P84; BD Pharmingen), anti-DO11.10 clonotypic TCR (KJ1-26; BD Pharmingen), anti-F4/80 (A3-1; Serotec), and anti-Ly51 (6C3; BioLegend). Hamster anti-mouse CD11c (HL-3) and mouse anti-mouse I-A^d (AMS-32.1) mAbs were purchased from BD Pharmingen. Rabbit anti-mouse CCR2 mAb and anti-mouse type IV collagen (Col IV) polyclonal Ab were purchased from Epitomics and LSL, respectively. Goat anti-mouse MCP-2 polyclonal Ab was purchased from Santa Cruz Biotechnology. Isotype-matched control IgGs for each rat and hamster mAbs were purchased from BD Pharmingen. Mouse, rabbit, and goat IgG (Sigma-Aldrich) served as controls.

Cell preparation

Thymus was digested in 0.6 mg/ml collagenase type IV (Sigma-Aldrich) and 25 Kunitz units/ml DNase I (Sigma-Aldrich) in RPMI 1640 (Sigma-Aldrich) at 37°C for 20 min. The low-density cells were further isolated from the resultant single-cell suspensions using Histopaque-1077 reagent (Sigma-Aldrich). PBMCs were isolated from whole blood using Histopaque-1083 reagent (Sigma-Aldrich). Bone marrow cells were washed out with cold RPMI 1640 medium from the femoral and tibial bones.

Flow cytometry (FCM)

The low-density cells from thymus, PBMCs, and bone marrow cells were stained with various combinations of fluorescent dye-conjugated or nonconjugated specific Abs in PBS supplemented with 2 mM EDTA and 3% FBS. For nonconjugated Abs, fluorescent-conjugated secondary Abs were used. After washing in PBS, expression of cell surface molecular markers was analyzed using a FACSCalibur (BD Biosciences) with CellQuest Pro software (BD Biosciences).

Histology and fluorescent immunohistochemistry

Thymic tissues were frozen in OCT compound (Sakura) and 6-μm-thick cryostat sections were stained with H&E. For immunofluorescence analysis, 6-μm-thick cryostat sections were fixed with cold acetone for 3 min and incubated with Protein Block Reagent (DakoCytomation) to block nonspecific binding. Then fluorescent immunostaining was done by the standard method (for details, see the figure legends). After washing with 0.05% Tween 20-PBS, slides were mounted in fluorescent mounting medium (DakoCytomation). Immunofluorescence was detected in a setting that excluded the nonspecific signal of the isotype control using a fluorescence microscope (BX50; Olympus) or confocal laser-scanning microscope (LSM510; Zeiss). DP Controller software (Olympus) and Zen 2007 software (Zeiss) were used for image processing.

RT-PCR

Total RNAs were extracted from tissues using a RNeasy Mini Kit (Qiagen) and then reverse-transcribed using SuperScript III First-Strand Synthesis System (Invitrogen). PCR was done using the cDNAs, 2.5 mM dNTP mix (Takara), TaqDNA polymerase (Takara), and the specific primer sets for the *GAPDH* gene (sense, 5′-CAC TGA GCA TCT CCC TCA CA-3′ and antisense, 5′-TGG GTG CAG CGA ACT TTA TT-3′), *CD45* gene (sense, 5′-AAG ACA GAG TGC AAA GGA GAC-3′ and antisense, 5′-TGT AGG TGT TTG CCC TGT GAC AAA GAC-3′), *keratin 8* gene (sense, 5′-ACG GTG AAC CAG AGC CTG T-3′ and antisense, 5′-CTC CAC TTG GTC TCC AGC AT-3′), *MCP-1* gene (sense, 5′-CCC ACT CAC CTG CTG CTA CT-3′ and antisense, 5′-TCT GGA CCC ATT CCT TCT TG-3′), *MCP-2* gene (sense, 5′-CAG TCA CCT GCT GCT TTC AT-3′ and antisense, 5′-ATA CCC TGC TTG GTC TGG AA-3′), and *MCP-3* gene (sense, 5′-AAA CAA AAG ATC CCC AAG AGG-3′ and antisense, 5′-CAC AGA CTT CCA TGC CCT TC-3′) for 30 cycles of 95°C for 30 s, 55°C for 30 s, and 72°C for 30 s.

Effects of a peptide Ag on DO11.10 clonotypic thymocytes

DO11.10-transgenic mice with or without *CCR2* gene deficiency were administered 200 μg of $OVA_{323-339}$ peptide (ABGENT) in PBS through the tail vein. To induce thymocyte deletion independently of Ag presentation, mice were injected i.p. with 50 μg of anti-CD3ε mAb (24). Two days after injection, thymocytes were collected and stained with the following combinations of Abs: anti-CD4, anti-CD8, and anti-DO11.10 or anti-CD4, anti-CD25, and anti-DO11.10 Abs. To detect apoptotic cells, thymocytes were stained using an Annexin V-FITC Apoptosis Detection Kit (Merck). After being stained, the cells were analyzed by FCM.

Trafficking of bone marrow-derived immature DCs injected into bone marrow

Bone marrow cells were cultured in RPMI 1640 medium supplemented with 10% FBS and mouse GM-CSF (R&D Systems) at a concentration of 20 ng/ml. An equal volume of culture medium of the same content was added at 4 days, and one-half of the medium was replaced with fresh culture medium at 7 days after the plating. Most bone marrow cells were differentiated into immature DCs as judged by morphological appearances at 10 days after the initiation of the culture. The resultant immature DCs were stained with 1 μM 5-chloromethylfluorescein diacetate (CMFDA; Invitrogen) dye and 1 million cells were injected into the tibial bone marrow cavity of each mouse. After the injection, low-density cells were obtained from thymus, lymph nodes, or PBMCs to determine the presence of CMFDA-stained DCs by using FCM.

Localization of the i.v. injected Ags

Alexa Fluor 488-conjugated OVA protein (OVA_{488}), Alexa Fluor 647-conjugated OVA protein (OVA_{647}) (Invitrogen), or mouse serum IgG (Sigma-Aldrich), which was conjugated with Alexa Fluor 647, using an Alexa Fluor 647 protein labeling kit (Invitrogen), was injected into the tail vein of mice. Thymic low-density cells and PBMCs were isolated at the indicated time points after OVA protein injection and were stained with anti-CD11c and anti-Sirpα Abs. Then the cells were analyzed by FCM. For the localization of the Ag uptake, cryostat sections of frozen thymic tissues were obtained from mice injected with OVA protein and were stained with anti-Sirpα, anti-CD11c, anti-I-A^d, anti-Ly51, or anti-Col IV Abs and were then observed by fluorescence microscope.

In vitro endocytosis assay

Low-density cells were isolated from the thymus and were incubated with 10 μg/ml OVA_{647} in RPMI 1640 at 37°C for 20 min. As a negative control, incubation was conducted on ice. Endocytosis by each thymic DC subset was analyzed by FCM after being stained with anti-CD11c and anti-Sirpα Abs. In some experiments, low-density cells were preincubated with 10 μM cytochalasin D (Cyt D; Sigma-Aldrich), an actin inhibitor (25), 100 mM ammonium chloride (NH_4Cl) (Wako), an inhibitor of the clathrin-dependent pathway (26), or 0.5 mg/ml mannan (Sigma-Aldrich) at 37°C for 15 min before incubation with OVA_{647} at 37°C for 20 min in the presence of fresh inhibitors.

Adoptive transfer of bone marrow cells

Bone marrow cells were obtained from WT or CCR2$^{-/-}$ mice and were stained with 2 μM CMFDA dye. Twenty million cells were injected into the tail vein of CCR2$^{-/-}$ mice. OVA_{647} was injected into the tail vein at 2 days after injection. Thymic low-density cells were isolated at 1 h after OVA protein injection, and the presence of donor-derived Sirpα$^+$ cDCs and their capability of Ag uptake were analyzed by FCM.

In vivo cell proliferation assay

Spleen mononuclear cells were isolated from WT or CCR2$^{-/-}$ mice and were labeled with 25 μM CFSE using a CellTrace CFSE Cell Proliferation Kit (Invitrogen). Ten million prelabeled cells were injected into the tail vein of WT mice. One day after injection, mice were immunized with total

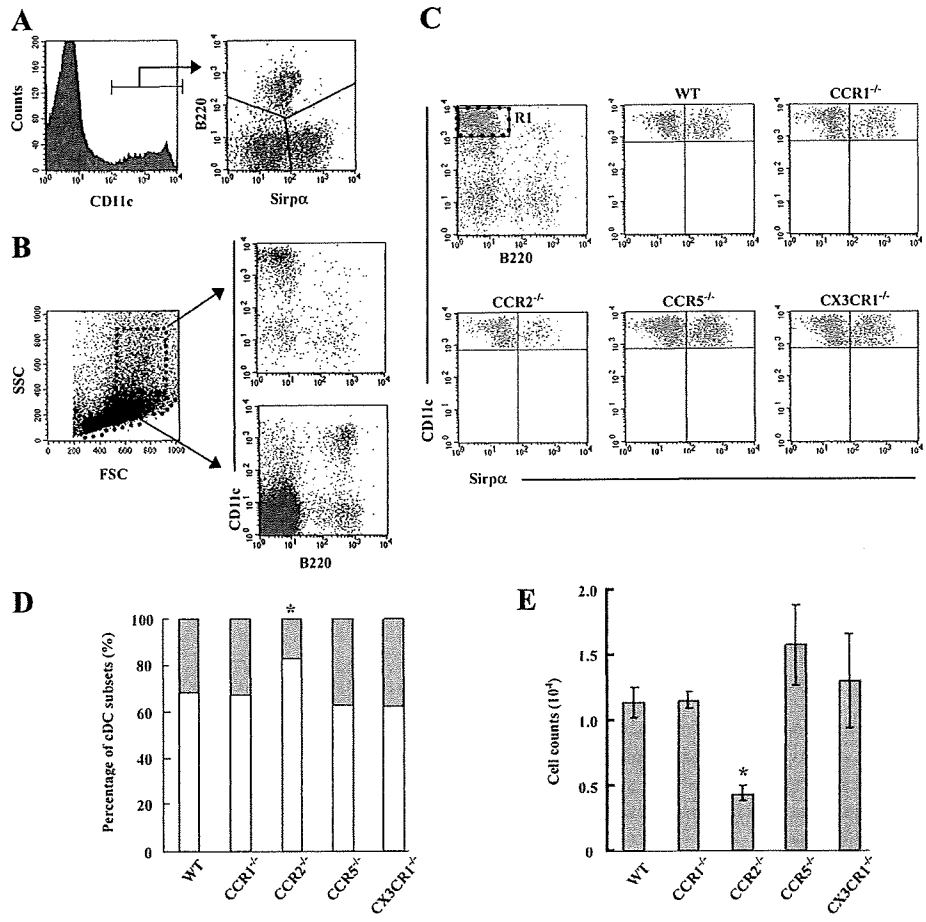

FIGURE 1. Effects of chemokine receptor deficiency on mouse thymic DC subsets. *A*, Low-density cells were isolated from WT mouse thymus and were stained with PE-conjugated anti-CD11c, allophycocyanin-conjugated anti-B220, and nonconjugated anti-Sirpα mAbs, followed by staining with FITC-conjugated mouse anti-rat IgG1. The CD11c$^+$ DC populations were gated to analyze the expression of Sirpα and B220. *B*, Thymic low-density cells were divided into two groups based on their FSC and SSC patterns, which are indicated by elliptic and square gates. Then DC subsets in each region were analyzed. *C*, Low-density cells were isolated from WT, CCR1$^{-/-}$, CCR2$^{-/-}$, CCR5$^{-/-}$, and CX3CR1$^{-/-}$ mice. The Sirpα$^-$ and Sirpα$^+$ subsets in FSC^{high} SSC^{high}CD11c^{high}B220$^-$ cDC populations gated with region 1 (R1) were compared among these mice. *D*, The ratio of two DC subsets (blank portion, Sirpα$^-$ subset; gray portion, Sirpα$^+$ subset) present in thymic cDC population was determined. Data represent the mean of three independent experiments. *E*, The numbers of Sirpα$^+$ DCs in the thymus. Data represent mean ± SD from three independent experiments. *, $p < 0.01$.

mouse serum protein emulsified in CFA. PBS in CFA was immunized as a control. Two days after immunization, lymphocytes were harvested from draining and nondraining lymph nodes and stained with anti-CD4 mAb. The percentage of CFSE-diluted divided cells was analyzed by FCM.

Statistical analysis

Data are represented as mean ± SD. Statistical significance was determined by one-way ANOVA followed by the Tukey-Kramer test. A value of $p < 0.05$ was considered statistically significant.

Results

Selective reduction of thymic Sirpα$^+$ cDCs in CCR2$^{-/-}$ mice

Consistent with a previous report (8), three distinct populations of thymic CD11c$^+$ DCs have been identified: B220$^+$ pDC, B220$^-$ Sirpα$^-$ cDC, and B220$^-$Sirpα$^+$ cDC subsets (Fig. 1*A*). cDC and pDC subsets were present mainly in the forward scatter (FSC^{high}), side scatter SSC^{high}, and SSC^{low} areas upon FCM, respectively (Fig. 1*B*). The pivotal role of chemokines in the trafficking of DCs prompted us to examine thymic DC subsets in mice deficient in chemokine receptor genes. Sirpα$^+$ DCs were markedly decreased in CCR2$^{-/-}$ mice, compared with WT mice, both in the relative (Fig. 1, *C* and *D*) and absolute number (Fig. 1*E*), whereas Sirpα$^-$ DC (Fig. 1*C*) and B220$^+$ pDC numbers (data not shown) were not changed in CCR2$^{-/-}$ mice. In contrast, no significant changes were observed on thymic cDC and pDC subsets in mice deficient in other chemokine receptors including CCR1, CCR5, and CX3CR1. Moreover, we did not observe any differences in thymic B220$^+$ B cell and F4/80$^+$ macrophage numbers between WT and CCR2$^{-/-}$ mice (data not shown). Microscopic studies of the thymus failed to reveal any morphological differences between WT and CCR2$^{-/-}$ mice in terms of the total cellularity, the distribution of thymocytes in each developmental stage, and the localization of Ly51$^+$ cortical thymic epithelial cells and I-A$^{d\ high}$ mTEC (supplemental Fig. S1[3]). Thus, CCR2$^{-/-}$ mice exhibit a selective decrease in the Sirpα$^+$ DC subset in thymus.

Attenuation of OVA$_{323-339}$ peptide-induced clonal deletion by CCR2 gene ablation

Sirpα$^+$ DCs are presumed to have the capacity to carry peripheral tissue Ags into the thymus (14). We next investigated the roles of Sirpα$^+$ DCs in thymus on taking in an i.v. administered Ag. PBS injection did not cause any changes in each developmental stage of thymocytes in DO11.10 and DO11.10/CCR2$^{-/-}$ mice (data not shown). On the contrary, i.v. administration of OVA$_{323-339}$ peptide markedly reduced the proportion and absolute number of clonotypic CD4/CD8 double-positive (DP) thymocytes in DO11.10 mice. *CCR2* gene ablation modestly attenuated this reduction (Fig. 2, *A–C*). OVA peptide injection consistently increased the proportion of annexin V$^+$ apoptotic cells in DO11.10 mouse thymus compared with that in DO11.10/CCR2$^{-/-}$ mice (Fig. 2*D*). In contrast, OVA peptide induced a modest increase in the number of DO11.10$^+$CD25$^+$CD4$^+$ regulatory T cell phenotype to similar extents in both DO11.10 and DO11.10/CCR2$^{-/-}$ thymus (Fig. 2*E*). Thus, decreased thymic Sirpα$^+$ DCs in CCR2$^{-/-}$ mice may be associated with a moderately impaired thymic negative selection. Moreover, following i.p. injection with anti-CD3 Ab (24), thymocytes were deleted to similar extents in DO11.10 and DO11.10/CCR2$^{-/-}$ mice

[3] The online version of this article contains supplemental material.

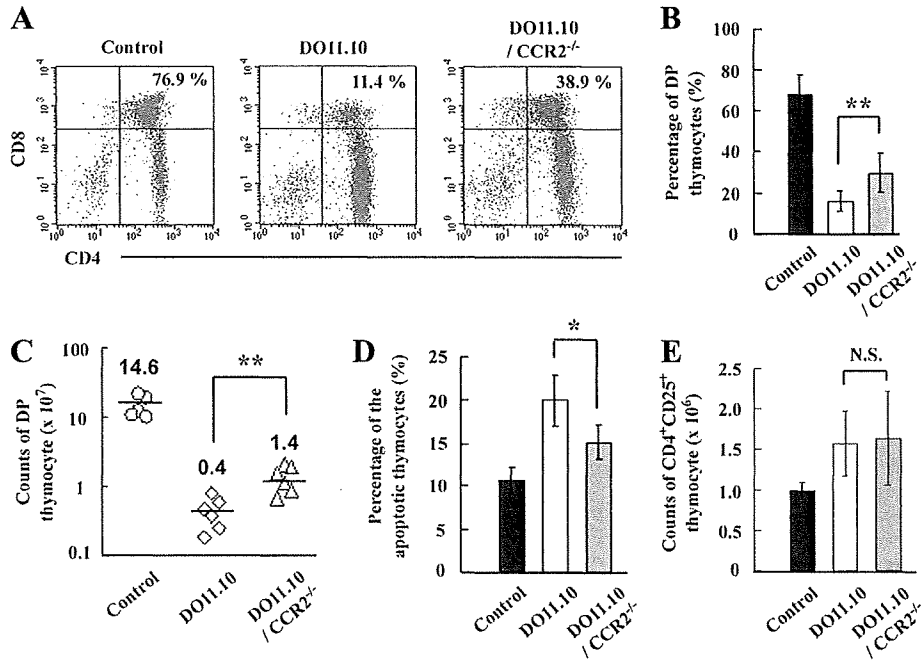

FIGURE 2. Induction of clonal deletion of DO11.10 clonotypic thymocytes. To induce the clonal deletion, 200 μg of $OVA_{323-339}$ peptide in PBS was injected into the tail vein of DO11.10-transgenic or DO11.10/$CCR2^{-/-}$ mice. PBS was injected as a control. DO11.10-transgenic TCR-expressing thymocytes were identified as KJ1-26-positive cells. *A*, Each developmental stage of thymocytes after $OVA_{323-339}$ peptide injection. Percentage of DP stage is shown in each panel. *B*, Percentage of DP stage of development; *C*, the number of DP thymocytes; *D*, percentage of the apoptotic thymocytes; and *E*, the number of $CD4^+$ $CD25^-$ thymocytes were determined on DO11.10 and DO11.10/$CCR2^{-/-}$ mice. Representative results from at least four independent experiments are shown in *A* while the mean ± SD was calculated on at least four independent experiments and are shown in *B–E*. *, $p < 0.05$ and **, $p < 0.01$. N.S., No significant difference.

(supplemental Fig. S2), indicating the absence of intrinsic defects of thymocytes in the absence of CCR2. These results collectively suggest that thymic Sirpα$^+$ DCs can contribute to intrathymic negative selection of a bloodstream-derived Ag without inducing regulatory T cells.

Thymic Sirpα$^+$ DCs can efficiently capture peripheral Ag from bloodstream

To elucidate the functions of thymic Sirpα$^+$ DCs more in detail, we determined their intrathymic localization. In thymi of WT mice, Sirpα was mainly detected on $CD11c^+$ DCs scattered in the thymic cortex (Fig. 3, *A* and *B*), but not on $CD11c^+$ DCs clustered in medulla, the predominating site of thymic $CD8\alpha^+$Sirpα$^-$ DCs. Moreover, most Sirpα$^+$ DCs were localized in close proximity to small vessels with single Col IV^+ basement membrane or inside perivascular regions (PVRs) separated by two Col IV^+ basement membranes in the cortex (Fig. 3*C*). The thymic DC population includes APCs crucially involved in the central tolerance system involving bloodstream C5 Ag (27). Furthermore, Sirpα$^+$ DCs are selectively localized in PVRs or in close proximity to small vessels, both essential components of the blood-thymus barrier (28). Hence, we hypothesized that this DC subset might be involved in Ag uptake from the bloodstream. To address this possibility, we treated WT mice i.v. with OVA_{647} and examined its uptake by thymic DCs. Intrathymic Sirpα$^+$ DCs, but not Sirpα$^-$ DCs, took up OVA protein in a dose-dependent manner (Fig. 4*A*), maintaining a stable level from 1 to 4 h after the injection and decreasing thereafter (Fig. 4*B*). Recently, it was reported that bloodstream DCs could efficiently capture and transport particulate bacteria into the spleen when particulate bacteria were i.v. injected (29). Indeed, bloodstream $CD11c^+$ cells rapidly disappeared from the peripheral blood after capturing OVA protein (Fig. 4*C*). By contrast, the uptake by intrathymic Sirpα$^+$ DCs reached a peak level at 15 min, decreasing to the stable level thereafter. Thus, there may be a remote possibility that circulating DCs migrated into the thymus after capturing OVA protein inside the bloodstream. Furthermore, in addition to an exogenous protein, intrathymic Sirpα$^+$ DCs also captured an endogenous serum protein, mouse IgG, which was conjugated with Alexa Fluor 647, when it was administered i.v. (supplemental Fig. S3). Thus, Sirpα$^+$ DCs can effectively capture peripheral Ags from the bloodstream across the blood-thymus barrier. This notion was further supported by the observation that Sirpα$^+$ DCs engulfed OVA protein with a higher efficiency than Sirpα$^-$ DCs when cultured in vitro with OVA_{647} (Fig. 4, *D* and *E*). Mannan from *Saccharomyces cerevisiae*, but not NH_4Cl or Cyt D from *Zygosporium mansonii*, markedly inhibited endocytosis of OVA protein by Sirpα$^-$ DCs (Fig. 4*F*, *upper panel*). On the contrary, uptake of OVA protein by Sirpα$^+$ DCs was markedly attenuated by NH_4Cl and Cyt D, but not mannan (Fig. 4*F*, *lower panel*). These observations suggest that thymic Sirpα$^+$ DCs can endocytose soluble Ags more efficiently than Sirpα$^-$ DCs, in a clathrin-dependent, but not mannose receptor-dependent manner.

Thymic Sirpα$^+$ DCs capture peripheral Ag inside PVRs or nearby small vessels, and then migrate into the cortical parenchyma

We examined sequentially intrathymic localization of OVA-derived signals after i.v. injection of OVA_{488}. By 0.5 h, OVA_{488}-derived signals were detected in Sirpα$^+$ cells (Fig. 5*A*), $CD11c^+$ DCs (Fig. 5*B*) and inside PVRs or in close proximity to small vessels (Fig. 5*C*). Although some signals remained nearby in small vessels, signals inside PVRs were obviously decreased at 6 h (Fig. 5*D*), as judged by the Col IV immunostaining pattern. At 18 h after the injection, OVA_{488}-derived signals were mainly scattered in the $Ly51^+$ cortical area but not in the $I\text{-}A^{d\ high}$ medullary area (Fig. 5*E*). Because OVA_{488}-derived signals were constantly detected in Sirpα$^+$ DCs at every time point (data not shown), these observations suggest that Sirpα$^+$ DCs initially capture bloodstream OVA protein inside PVRs or in nearby small vessels and then migrate into the cortical parenchyma. To examine the process of migration more in detail, OVA_{647} (blue) and OVA_{488} (green) were i.v. injected sequentially with an interval of either 6 or 18 h as shown in Fig. 5*F*. When OVA_{488} was injected 6 h after OVA_{647}, double-positive $CD11c^{high}$ DCs were evidently detected (8.1%), while single-positive cells were sparse (Fig. 5*F*, *left upper panel*). Even at 18 h after the injection, double-positive $CD11c^{high}$ DCs were still

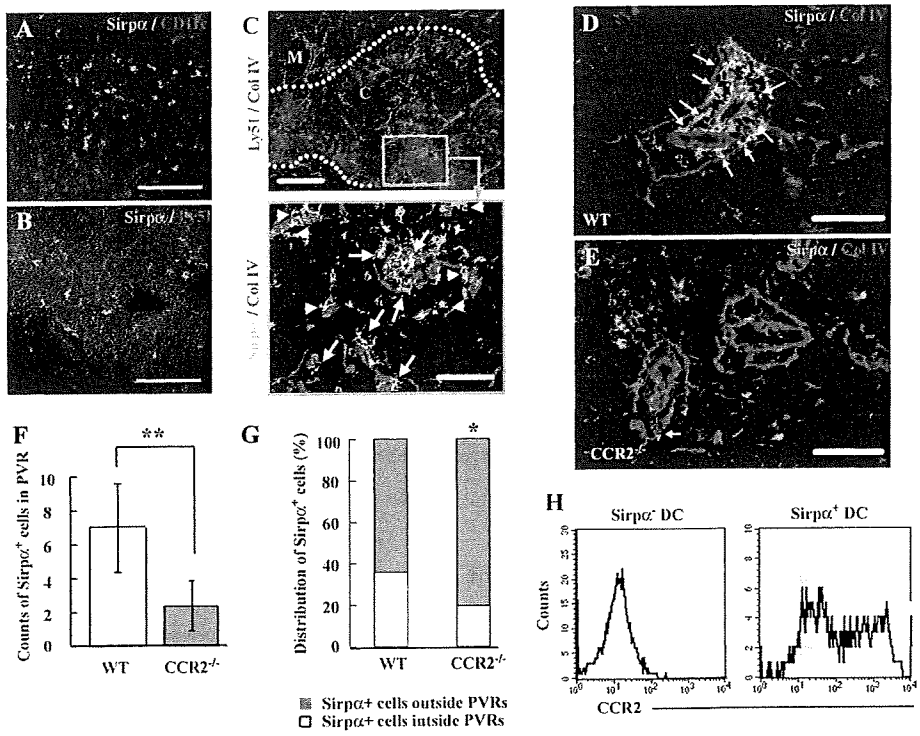

FIGURE 3. Localization of thymic Sirpα$^+$ DCs. Double-color fluorescence immunostaining for Sirpα (green) and CD11c (red; *A*), Ly51 (red; *B*), or Col IV (red; *D* and *E*). *C*, Triple-color fluorescent immunostaining for Sirpα (green), Ly51 (red), and Col IV (blue). Low magnification image for Ly51 and Col IV is shown in the *upper panel*. A green square in the *upper panel* is observed at a higher magnification for Col IV and Sirpα expression and is shown in the *lower panel*. Dashed lines indicate the boundary between cortex (C) and medulla (M). Arrowheads in *C* and arrows in *C–E* indicate Sirpα$^+$ cells interacting with small vessels and inside the PVRs, respectively. *A–D*, WT thymus. *E*, CCR2$^{-/-}$ thymus. Representative results from at least two independent experiments are shown here. Scale bars: *A* and *B*, 100 μm; *upper panel* of *C*, 200 μm; *lower panel* of *C–E*, 50 μm. *F* and *G*, At least five photographs in the central regions of the PVRs were taken at ×200 magnification in each tissue sample. The numbers of Sirpα$^+$ cells inside the PVRs were determined and data represent mean ± SD of three independent experiments. **, $p < 0.01$. *F*, The proportion of Sirpα$^+$ cells inside the PVRs to outside was calculated and data represent the mean of three independent experiments. *, $p < 0.05$ (*G*). *H*, CCR2 expression on CD11c^{high}Sirpα$^-$ or Sirpα$^+$ cDCs. Gray-filled and black-open histograms indicate the results from isotype control and specific mAb for CCR2, respectively. Representative results from three independent experiments are shown here.

present (3.2%) with substantial numbers of OVA_{488}-derived signal single-positive (3.9%) or OVA_{647}-derived signal single-positive cells (2.3%; Fig. 5*F*, *left lower panel*). Thus, CD11c^{high} DCs with Sirpα expression can persistently be in close interaction with the bloodstream while they are migrating into cortical parenchyma (Fig. 5*G*).

Depressed migration of Sirpα$^+$ DCs and their aberrant intrathymic localization in CCR2$^{-/-}$ mice

It is possible that a decreased intrathymic Sirpα$^+$ DC number may account for the defect in their migration in CCR2$^{-/-}$ mice, because the thymic Sirpα$^+$ cDC subset is presumed to migrate from the bloodstream (14). Most CD11c$^+$B220$^-$ DCs in peripheral blood and bone marrow expressed abundantly Sirpα (supplemental Fig. S4), similarly as observed on thymic Sirpα$^+$ DCs, and this population expressed CCR2 (supplemental Fig. S5). CCR2$^{-/-}$ mice exhibited a moderate reduction in CD11c$^+$B220$^-$ DCs in peripheral blood, but not bone marrow (Fig. 6, *A* and *B*). This suggests a possible defect in the migration of CD11c$^+$B220$^-$ DCs from bone marrow in CCR2$^{-/-}$ mice. To test this possibility, bone marrow cells were induced to differentiate to DCs with in vitro GM-CSF stimulation, labeled with CMFDA, and injected into bone marrow of WT mice (Fig. 6*C*, *upper illustration*). Under these conditions, >80% of injected cells expressed CD11c, Sirpα, and CCR2, but not B220 (supplemental Figs. S4 and S5). WT-derived DCs appeared in peripheral blood rapidly within 2 h after the intra-bone marrow injection, whereas CCR2$^{-/-}$ mouse-derived DCs migrated into peripheral blood less efficiently (Fig. 6, *C* and *D*). Interestingly, CD11c$^+$B220$^-$Sirpα$^+$ DCs appeared in thymus by 6 h after intra-bone marrow injection (Fig. 6*E*). These observations suggest that CCR2-mediated signals were critical of the migration of Sirpα$^+$ DCs from bone marrow into the thymus. Moreover, Sirpα$^+$ DCs were markedly decreased in PVRs of CCR2$^{-/-}$ thymus compared with those of WT thymus (WT mice, 7.0 ± 2.6/site; CCR2$^{-/-}$ mice, 2.3 ± 1.5/site; Fig. 3, *D–F*). Furthermore, the decrease was more evident in the region inside the PVRs compared with that outside the PVRs (Fig. 3*G*). CCR2 was expressed also by a portion of intrathymic Sirpα$^+$ DCs, but not Sirpα$^-$ DCs (Fig. 3*H*). Three mouse chemokines, MCP-1, MCP-2, and MCP-3, can bind to CCR2 (30). Among these chemokines, only MCP-2 mRNA was constitutively expressed in thymus, particularly keratin 8-positive thymic stroma, but not CD45-positive thymocytes (Fig. 7, *A* and *B*). Moreover, MCP-2 immunoreactivities were consistently detected inside the PVRs (Fig. 7*C*, *upper panels*) and on Sirpα$^+$ cells in the PVRs (Fig. 7*C*, *lower panels*). Thus, it is probable that the CCR2-MCP-2 interaction can contribute to intrathymic localization of Sirpα$^+$ DCs, particularly in the PVRs.

Defective Ag uptake by Sirpα$^+$ DCs in CCR2$^{-/-}$ mice

Because the PVR was proved to be a main location of the uptake of circulating Ags, we further examined the effects of CCR2

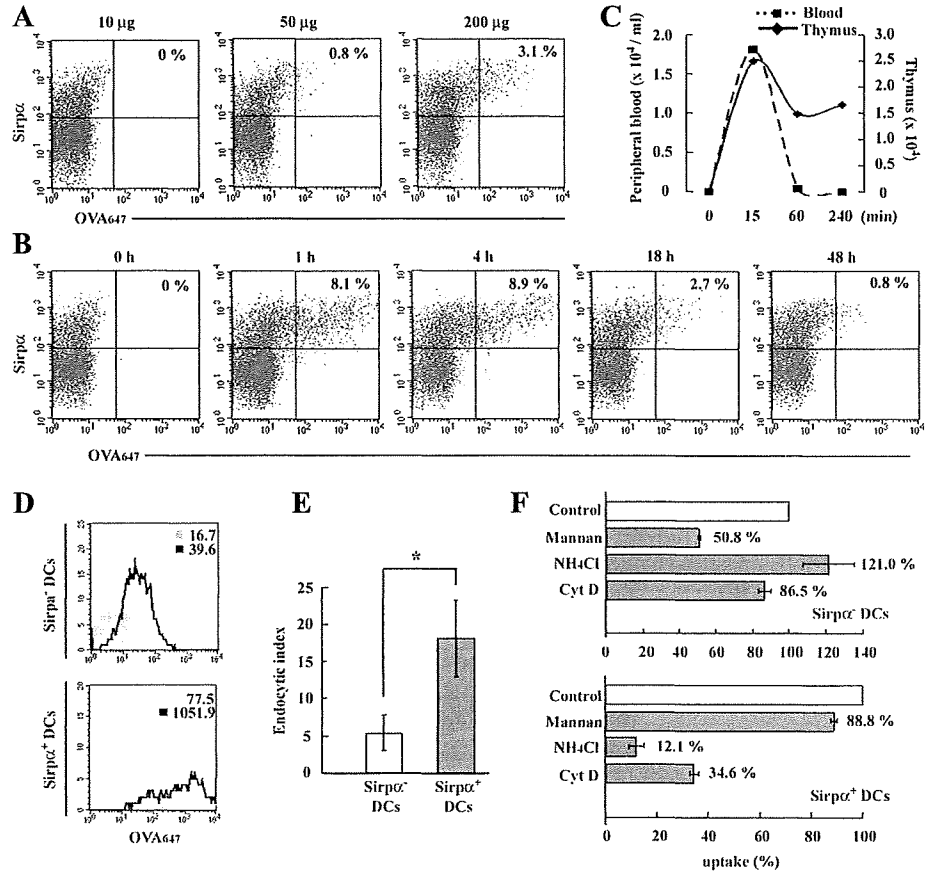

FIGURE 4. Uptake of bloodstream Ag by thymic Sirpα+ DCs. *A*, At 18 h after injection with OVA_{647} at the indicated doses, low-density cells were isolated from WT thymus and were stained with anti-CD11c and anti-Sirpα mAbs. Then the uptake of OVA_{647} in the $CD11c^{high}$ DC population was analyzed. *B*, Uptake of OVA_{647} at the indicated time points. OVA_{647} (200 μg) was injected into the tail vein. Percentage of $Sirp\alpha^{+}OVA_{647}^{+}$ region is shown in each panel of *A* and *B*. Representative results from three independent experiments are shown. *C*, Time kinetics of the numbers of DCs capturing OVA protein in the peripheral blood (broken line) and thymus (solid line). *D*, In vitro endocytosis of OVA_{647} by $CD11c^{high}Sirp\alpha^{-}$ and $CD11c^{high}Sirp\alpha^{+}$ cDCs are shown in the *upper* and *lower panels*, respectively. Gray-filled and black-open histograms indicate the results obtained when the cells were incubated at 0 and 37°C, respectively. Numbers in each panel indicates mean fluorescence intensity for OVA_{647} captured. Representative results from three independent experiments are shown here. *E*, Endocytic index in $Sirp\alpha^{-}$ and $Sirp\alpha^{+}$ cDCs. Endocytic index was calculated as mean fluorescence intensity at 37°C/mean fluorescence intensity at 0°C. Mean ± SD were calculated from three independent experiments and are shown here. *, $p < 0.01$. *F*, The effects of various agents on endocytosis. Uptake in the presence of each inhibitor is shown as the percentage of total uptake in the absence of any inhibitors. Means were calculated from three independent experiments and are shown here.

deficiency on the capability of $Sirp\alpha^{+}$ DCs to uptake Ags from the bloodstream. Indeed, when OVA_{647} was injected i.v., $CCR2^{-/-}$ mice exhibited a reduced proportion of intrathymic DCs capturing OVA protein compared with WT mice (Fig. 8, *A* and *B*). Moreover, after the OVA_{647} injection, $Sirp\alpha^{+}$ DCs of WT mice contained a substantial proportion of OVA^{high} cells, which represent the cells with a higher uptake of OVA protein, and this population was markedly reduced in $CCR2^{-/-}$ mice (Fig. 8, *C* and *D*). Moreover, among $Sirp\alpha^{+}$ DCs, the CCR2-expressing population was a main cell type which captured OVA protein (Fig. 8*E*). CMFDA-labeled WT mouse-derived bone marrow cells appeared in thymus 2 days after the adoptive transfer to CCR2-deficient mice and a substantial proportion of these stained cells expressed CD11c and Sirpα simultaneously (Fig. 8*F*). $Sirp\alpha^{+}CD11c^{+}$ DCs appeared in thymus similarly when CMFDA-labeled CCR2-deficient mouse-derived bone marrow cells were adoptively transferred (data not shown). When OVA_{647} was injected i.v. 2 days after the adoptive transfer, WT donor-derived $Sirp\alpha^{+}CD11c^{+}$ DCs captured OVA protein more efficiently than CCR2-deficient DCs in the CCR2-deficient thymus (Fig. 8*G*). Thus, CCR2-mediated signals may at least partially regulate the function of $Sirp\alpha^{+}$ DCs to uptake Ag from the bloodstream (supplemental Fig. S6).

Accumulation of autoreactive T cells against serum Ags in the periphery of $CCR2^{-/-}$ mice

We observed that $CCR2^{-/-}$ mice did not exhibit any signs suggestive of autoimmune disorders until 1 year after the birth (our unpublished data). Hence, we examined whether autoreactive T cells against certain self-Ags in the bloodstream accumulated in the periphery of $CCR2^{-/-}$ mice. We examined the accumulation of autoreactive T cells in the draining lymph nodes in WT mice that received CFSE-labeled WT or $CCR2^{-/-}$ mouse-derived splenocytes and were subsequently immunized with mouse serum emulsified in CFA. Immunization with total serum protein increased the cell division of $CCR2^{-/-}$ mouse-derived $CD4^{+}$ T cells inside draining lymph nodes (10.6%) to a greater extent than immunization with PBS (4.3%; Fig. 9*A*). Moreover, $CD4^{+}$ T cell division was significantly increased in the recipients of $CCR2^{-/-}$ mouse-derived splenocytes compared with the recipients of WT mouse-derived splenocytes (Fig. 9*B*). Thus, the lack of CCR2 can

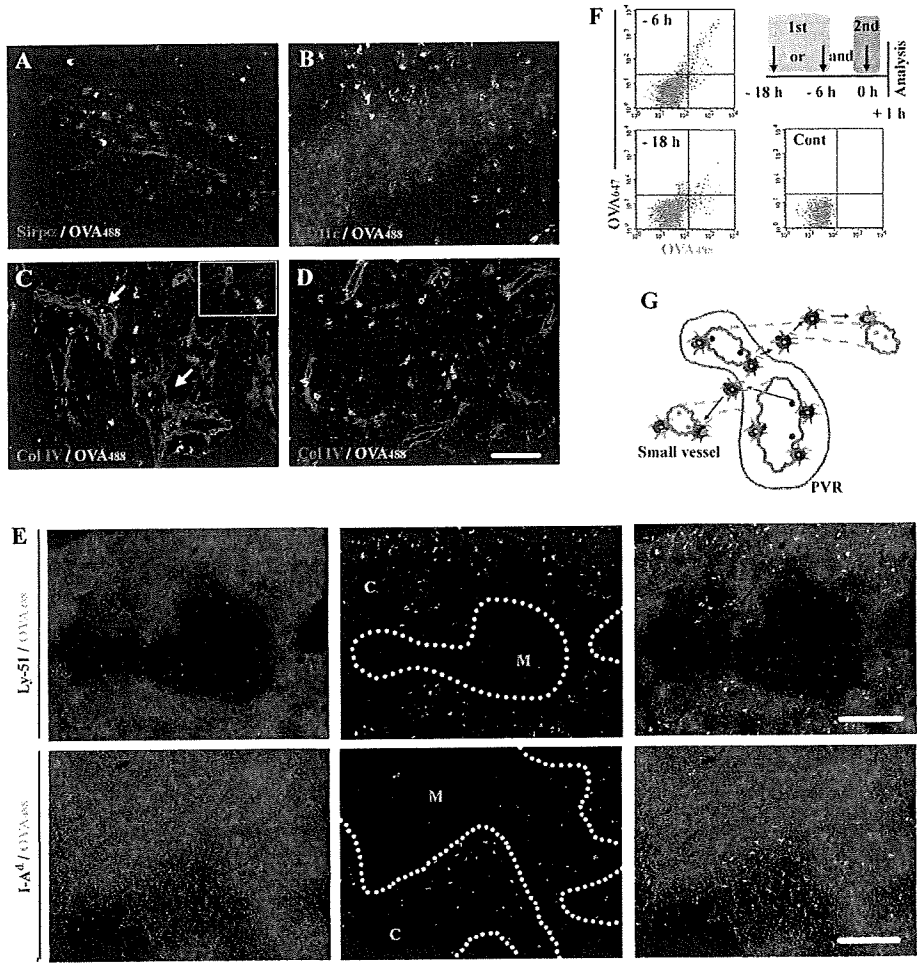

FIGURE 5. Localization of i.v. injected Ag in thymus. *A–C*, Thymic tissues were obtained 0.5 h after injection of OVA_{488} and were stained to obtain a double-color fluorescent image with the combination of OVA_{488} (green) and (*A*) Sirpα (red), (*B*) CD11c (red), or (*C*) Col IV (red). Arrows in *C* indicate the cells with captured OVA_{488} inside the PVRs. The image showing the cells capturing OVA_{488} in close proximity to small vessels is an *inset* in *C*. *D*, A double-color fluorescent image for OVA_{488} (green) and Col IV (red) at 6 h after OVA injection. Scale bars, 100 μm. *E*, A double-color fluorescent image with the combination of OVA_{488} (green) and Ly51 (red) or I-A^d (red) at 18 h after injection is shown in the *upper* and *lower panels*, respectively. The merged images are shown in the *right panels*. Dashed lines indicate the boundary between cortex (C) and medulla (M). Scale bars, 200 μm. *F*, OVA_{647} and OVA_{488} were i.v. injected consequently with an interval of either 6 or 18 h, illustrated in *upper right panel* in *F*. Uptake of OVA protein by CD11c^{high} DC population isolated after double injection with an interval of either 6 or 18 h is shown in the *left upper* and *lower panels*, respectively. Autofluorescence for each parameter in the CD11c^{high} DC population without injection is shown as a control. Representative results from three independent experiments are shown here. *G*, Presumed intrathymic trafficking modes of Sirpα^- DCs, combined with the Ag uptake. Blue and green particles indicate OVA_{647} and OVA_{488}, respectively.

result in enhanced accumulation of autoreactive T cells against serum self-Ags.

Discussion

Mouse thymus CD11c$^+$ cDCs can be classified into two populations, a major CD8α^+ and a minor CD8α^- one (31). CD8α^- cDCs can pick up CD8$\alpha\beta$ heterodimer from thymocytes and retain them on the cell surface, thus precluding the use of CD8α as a reliable marker to distinguish these two populations. Wu and Shortman (8) observed that CD8α^- but not CD8α^+ cDCs simultaneously express the Sirpα molecule and proposed the use of Sirpα as a marker of this minor cDC population. Concomitantly, it was proposed that the interaction between thymocytes and DCs in thymic cortex can also have profound effects on positive selection (32). Likewise, McCaughtry et al. (33) observed that clonal deletion of autoreactive thymocytes requires the stimuli from rare CD11c$^+$ cortical DCs. Given the unique localization of Sirpα^+ DCs confined to the cortex, these observations suggest the potential involvement of Sirpα^+ DCs in central tolerance, but their small number hinders the isolation for a detailed analysis of Sirpα^+ DC function.

A partial but selective reduction in intrathymic Sirpα^+ cDCs in CCR2$^{-/-}$ mice prompted us to investigate the thymic selection process in WT and CCR2$^{-/-}$ mice to elucidate the role of intrathymic Sirpα^+ cDCs in the process. When DO11.10 TCR-transgenic mice were administered immunogenic $OVA_{323-339}$ peptide i.v., *CCR2* gene ablation partially attenuated the clonal negative deletion by apoptosis of the DO11.10$^+$ DP thymocyte population. Intraperitoneal injection of anti-CD3 Ab deleted thymocytes to similar extents in WT and CCR2$^{-/-}$ mice, excluding the possibility that CCR2 deficiency impaired the apoptotic response of thymocytes. Negative selection can be exerted by various types of APCs including Sirpα^- cDCs, B cells, macrophages, cortical thymic epithelial cells, and mTEC in addition to Sirpα^+ cDCs. We

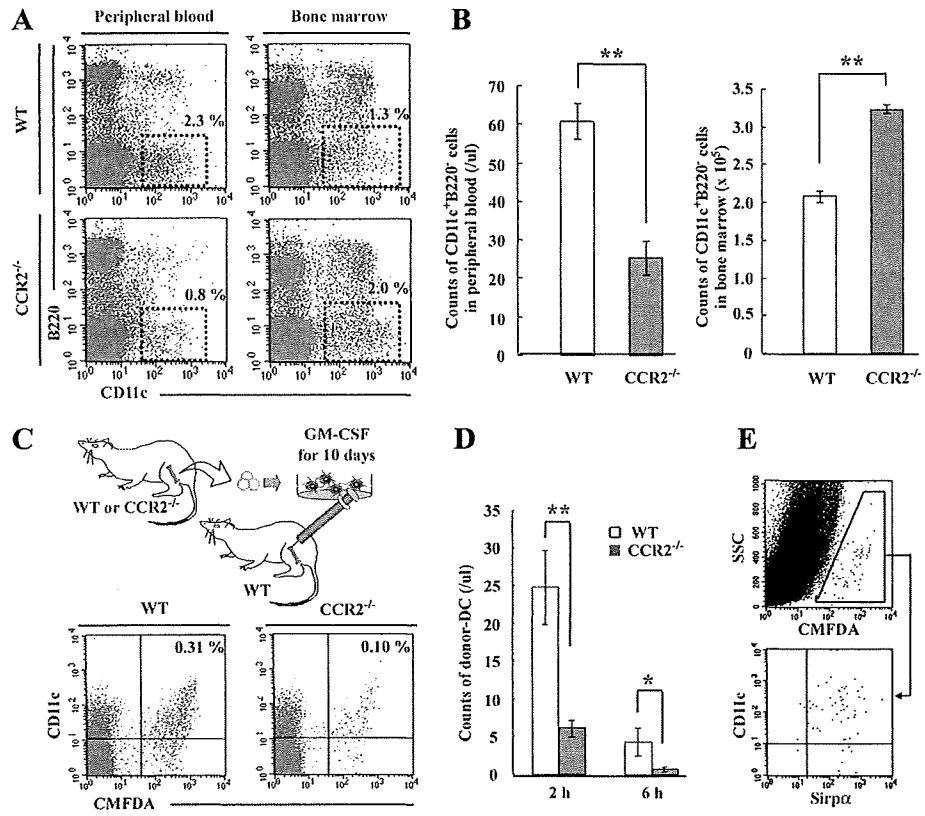

FIGURE 6. Mobilization of Sirpα^{+} DCs from bone marrow. *A* and *B*, PBMCs and bone marrow cells isolated from femur bone marrow were stained with anti-CD11c and anti-B220 mAbs. Proportion (*A*) and the numbers (*B*) of CD11c^{-}B220^{-} cells gated with the dot squares were determined on peripheral blood and bone marrow in CCR2$^{-/-}$ and WT mice. Percentage of gated cells is shown in each panel of *A*. Mean ± SD were calculated from three independent experiments and are shown here. *C*, The image of experimental procedure of "trafficking of bone marrow-derived DCs" was illustrated and is shown in the *upper panel*. PBMCs were isolated from the recipients 2 h after injection and stained with anti-CD11c mAb. Egress of CCR2$^{-/-}$ bone marrow-derived DCs into peripheral blood was compared with WT DCs. Percentage of donor DCs in CMFDA^{+}CD11c^{+} region is shown in each panel. *D*, The numbers of donor-derived DCs in peripheral blood were determined 2 and 6 h after injection. Mean ± SD calculated from five independent experiments are shown here. *, $p < 0.05$ and **, $p < 0.01$. *E*, One × 10^7 WT bone marrow cell-derived DCs were injected into both the right and left tibial cavity. Six hours after injection, expression of Sirpα and CD11c on intrathymic migrated CMFDA^{+} donor cells was analyzed by FCM. Representative results from four independent experiments are shown here.

failed to detect any apparent differences in other APC populations than Sirpα^{+} cDCs between WT and CCR2$^{-/-}$ mice. Thus, it is unlikely that reduced negative selection in CCR2$^{-/-}$ mice can be ascribed to the changes in these cell populations. Furthermore, accumulating evidence implicates intrathymic CD4^{+}CD25^{+} regulatory T cells as an essential cell component in central tolerance.

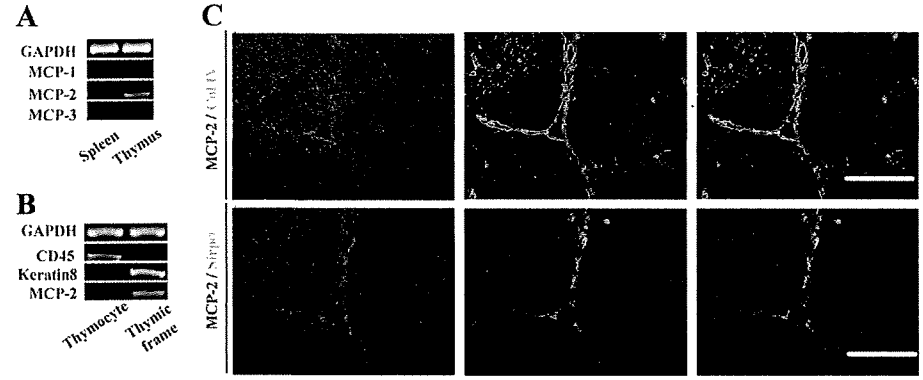

FIGURE 7. Expression of CCR2 ligands in thymus under physiological condition. *A*, Total RNAs were extracted from thymus and spleen of WT mice. Expression of CCR2 ligands, MCP-1, MCP-2, and MCP-3, was determined by RT-PCR. GAPDH served as an internal positive control. *B*, Thymic tissues were mechanically disrupted and fractionated into thymocyte and thymic stromal components. MCP-2 transcripts were determined on these two fractions by RT-PCR. CD45 and keratin 8 served as positive control for the thymocyte and thymic stromal fraction, respectively. *C*, Double-color fluorescent immunostaining for MCP-2 (red) and Col IV (green) or MCP-2 (red) and Sirpα (green) in the thymic tissue sections are shown in the *upper* and *lower panels*, respectively. The merged images are shown in the *right panels*. Representative results from three independent animals are shown here. Scale bars, 100 μm.

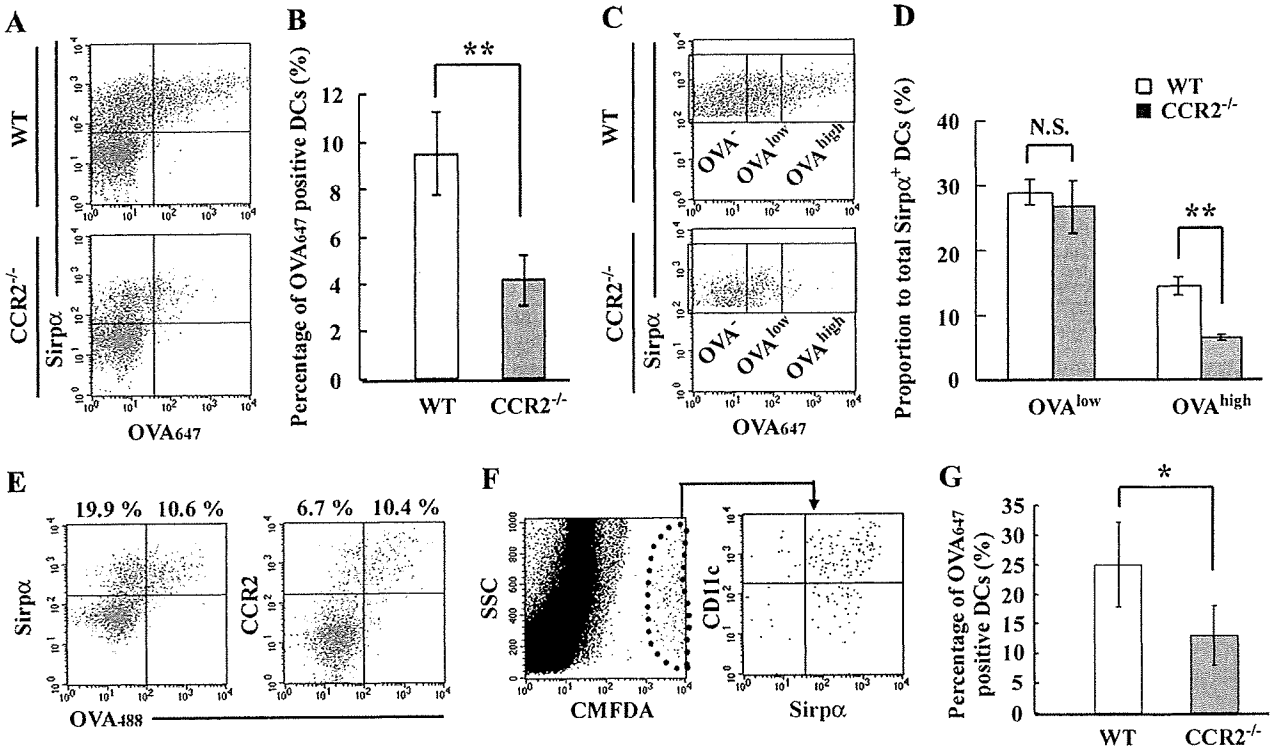

FIGURE 8. Effects of CCR2 deficiency on Ag uptake by thymic Sirpα^+ DCs. *A*, The uptake of OVA_{647} in the CCR2$^{-/-}$ CD11c^{high} DC population at 4 h after i.v. injection was compared with WT-derived cells. *B*, Percentage of DCs capturing OVA_{647} in the CD11c^{high} DC population. Mean ± SD were calculated from five independent experiments and are shown here. **, $p < 0.01$ *C*, Sirpα^+ DCs derived from WT and CCR2$^{-/-}$ thymus were separated into three groups according to the efficiency of OVA_{647} uptake, OVA$^-$; DCs without capturing OVA_{647}, OVA^{low}; DCs capturing OVA_{647} with a low efficiency, and OVA^{high}; and DCs capturing OVA_{647} with a high efficiency. *D*, Percentage of OVA^{low} and OVA^{high} in WT and the CCR2$^{-/-}$ Sirpα^- DC population. Mean ± SD were calculated from five independent experiments and are shown here. **, $p < 0.01$; N.S., no significant difference. *E*, OVA_{488} was i.v. injected into WT mice. One hour after injection, low-density cells were stained with anti-CD11c and anti-Sirpα or anti-CCR2 mAbs. The uptake of OVA_{488} and expression of Sirpα or CCR2 in the CD11c^{high} DC population are shown. Percentage of Sirpα^+OVA$_{488}^+$ and OVA_{488}^-, or CCR2$^+$OVA$_{488}^-$ and OVA_{488}^- regions are shown in the *left* or *right panel*. Representative results from three independent experiments are shown here. *F*, Migration of Sirpα^+ DCs into the thymus at 2 days after i.v. injection of CMFDA-labeled WT bone marrow cells into CCR2$^{-/-}$ mice. Expression of CD11c and Sirpα on CMFDA$^+$ donor-derived cells is shown in the *right panel*. Representative results from three independent experiments are shown here. *G*, OVA_{647} was i.v. injected into CCR2$^{-/-}$ mice at 2 days after injection of bone marrow cells. Percentage of WT and CCR2$^{-/-}$ donor-derived DCs capturing OVA_{647} in the CMFDA$^+$CD11c^{high} region are shown. Mean ± SD were calculated from four independent experiments and are shown here. *, $p < 0.05$.

Indeed, Proietto et al. (14) recently reported the capability of Sirpα^+ cDCs to induce the differentiation of regulatory T cells in vitro. However, OVA peptide injection induced the differentiation of regulatory T cells to similar extents in both DO11.10 and DO11.10/CCR2$^{-/-}$ thymus. Thus, it is probable that CCR2 deficiency reduced modestly intrathymic Sirpα^+ DCs without affecting regulatory cell induction and partially attenuated negative selection in vivo.

It remains elusive on the trafficking modes of Sirpα^+ DCs. In CCR2$^{-/-}$ mice, Sirpα^+ DCs were decreased moderately in peripheral blood and thymus, but were increased in bone marrow. Considering that CCR2 signaling can regulate the mobilization of monocytes from bone marrow to peripheral blood (34, 35), these observations raised the possibility of a defect in the trafficking of Sirpα^+ DCs from bone marrow in CCR2$^{-/-}$ mice. Indeed, WT mouse-derived Sirpα^+ DCs, injected into bone marrow, appeared first in peripheral blood and then the thymus. On the contrary, CCR2$^{-/-}$ mouse-derived Sirpα^+ DCs exhibited impairment in the egress from bone marrow to peripheral blood. These observations suggest that bone marrow-derived Sirpα^+ DCs migrated to peripheral blood in response to CCR2-mediated signals and subsequently traffic to the thymus.

In the thymus, Sirpα^+ DCs were characteristically localized in close proximity to small blood vessels and inside the PVRs, sites which are compartmentalized by a vascular basement membrane and a border membrane separating them from the thymic parenchyma (36). It is of note that Sirpα^+ cells in the PVRs were markedly decreased in CCR2$^{-/-}$ mice to a greater extent than the decrease in total Sirpα^+ cell number. Thus, intrathymic CCR2 signaling can regulate their unique localization. This notion was supported by the observation that MCP-2, a potential ligand for CCR2, was constitutively detected in the PVRs, where Sirpα^+ DCs were present.

PVRs can provide a pathway for hematopoietic progenitor cells and mature T cells to traverse from the bloodstream to the thymic parenchyma (36) and are presumed to constitute the blood-thymus barrier, which can protect the thymic parenchyma from bloodstream-derived macromolecules (28). Thus, the unique localization of Sirpα^+ cDCs in the thymus suggested their potential interactions with bloodstream-derived Ag. This assumption was strengthened by our present observation that intrathymic Sirpα^+ cDCs rapidly and specifically captured OVA protein and serum IgG following i.v. injection. Moreover, injected Ags were initially detected inside PVRs or in nearby small vessels and were subsequently in the cortical parenchyme, and the injected Ag-derived

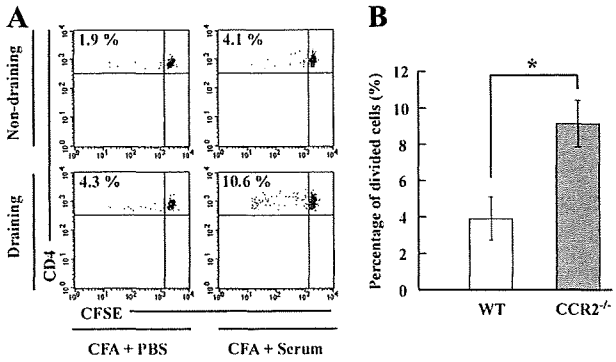

FIGURE 9. Accumulation of autoreactive T cells against serum Ags in the spleen. Spleen mononuclear cells were isolated from WT or CCR2$^{-/-}$ mice and i.v. injected into WT mice after labeling with CFSE. *A*, Recipients of CCR2$^{-/-}$ mouse-derived splenocytes were immunized with total mouse serum or PBS emulsified in CFA at 1 day after injection. Four days after, draining and nondraining lymph nodes were harvested and division of CFSE$^+$ donor-derived CD4$^-$ T cells was analyzed by FCM. Representative results from three independent experiments are shown here. *B*, Percentage of divided CD4$^+$ T cells was determined in the draining lymph nodes of the recipients of either WT-derived or CCR2$^{-/-}$ donor-derived splenocytes when the recipients were immunized with mouse serum emulsified in CFA. Mean ± SD were calculated from three independent experiments and are shown here. *, $p < 0.01$.

signals were consistently colocalized with CD11c and Sirpα. Thus, after CD11c$^+$Sirpα$^+$ cDCs, located around the PVRs, capture the Ags, they presumably move to cortical parenchyme to educate T cells. Indeed, CCR2$^{-/-}$ thymus-derived Sirpα$^+$ DCs exhibited a reduced capacity to uptake OVA. The lack of CCR2 can hinder the proper intrathymic localization of Sirpα$^+$ DCs and their distinctive function, Ag uptake from bloodstream, thereby reducing Ag presentation in the cortical parenchyma and subsequent negative selection against a blood-borne Ag. This hypothesis is supported by our observation in that CD4$^+$ T cells reactive to certain serum self-Ags accumulated in the periphery of the recipients of CCR2$^{-/-}$ mouse-derived splenocytes to a greater extent than the recipients of WT mouse-derived splenocytes.

DCs can uptake free soluble Ags, in three distinct manners, by clathrin-mediated endocytosis, nonclathrin/caveolae endocytosis, and macropinocytosis (25). Thymic Sirpα$^+$ cDCs could endocytose OVA Ags more efficiently than thymic Sirpα$^-$ cDCs when they were cultured in vitro with OVA Ags. Furthermore, NH_4Cl, an inhibitor of clathrin-mediated endocytosis (26), markedly inhibited OVA endocytosis by Sirpα$^+$ cDCs, but not by Sirpα$^-$ cDCs. On the contrary, OVA protein endocytosis by Sirpα$^-$ DCs was partially inhibited by mannan, whereas mannan had few effects on OVA protein endocytosis by Sirpα$^+$ DCs. These observations suggest that thymic Sirpα$^+$ cDCs characteristically can efficiently endocytose Ags in a manner distinct from thymic Sirpα$^-$ cDCs.

Balazs et al. (29) reported that bloodstream DCs could efficiently capture and transport particulate bacteria into the spleen when particulate bacteria were i.v. injected. We also observed that CD11c$^+$ DCs rapidly disappeared from peripheral blood after uptake of i.v. injected OVA protein. Given the capacity of CD11c$^+$ DCs to move rapidly from blood to thymus, blood CD11c$^+$ DCs may migrate into thymus after capturing the i.v. injected Ag. However, Ag-capturing DCs appeared very rapidly in the thymus, reaching maximal levels before disappearance of Ag-capturing circulating DCs from the peripheral blood. Furthermore, when OVA protein was injected i.v. into mice that contained bloodstream DCs labeled with fluorescent-conjugated latex beads, latex-labeled DCs did not appear in the thymus (our unpublished data). Thus, it is remotely possible that bloodstream DCs captured OVA protein and subsequently migrated into thymus.

In this study, we identified the unique intrathymic localization and functions of thymic Sirpα$^+$ DCs that are involved in negative selection, particularly against blood-borne Ags. Serum protein can also induce negative selection in thymus (27, 37) but the molecular and cellular mechanisms remain to be elucidated. Because Sirpα$^+$ cDCs can uptake serum protein such as IgG, these cells may induce central tolerance to blood-borne-derived Ags, in addition to Ags presented by the well-characterized intrathymic AIRE-mediated pathway.

We have shown that CCR2-mediated signals can regulate various biological aspects of Sirpα$^+$ DCs such as their appropriate intrathymic localization and Ag uptake capacity. It is widely held that CCR2 might be a potential therapeutic target for several autoimmune disorders. However, because CCR2-mediated signals may contribute to thymic negative selection against blood-borne Ags, CCR2 blockade may aggravate autoimmune disorders similar to the observation on the murine collagen-induced arthritis model (38). Moreover, Lauritzsen et al (39) reported that proteins secreted from tumor cells into peripheral blood were transported into the thymus to eventually cause clonal deletion of tumor Ag-specific T cell repertoires. Given the potential capacity of intrathymic Sirpα$^+$ DCs to capture blood-borne Ags, they may have a role in the development of tumor tolerance. Because human thymus contains DCs with similar phenotypes and intrathymic localization as Sirpα$^+$ cDCs (40), a more detailed elucidation of the functions of Sirpα$^+$ cDCs may provide us with useful insights to develop a better therapeutic strategy for cancer and stem cell transplantation as well as autoimmune disorders.

Acknowledgments

We express our gratitude to Drs. Joost J. Oppenheim (National Cancer Institute-Frederick, Frederick, MD) and Nobuyuki Onai (Akita University, Akita, Japan), and Yi Zhang (University of Michigan, Ann Arbor, MI) for critical review of this manuscript. We thank Drs. William Kuziel, Kouji Matsushima, and Philip Murphy for providing us with CCR2-, CCR5-, and CCR1- and CX3CR1-deficient mice, respectively.

Disclosures

The authors have no financial conflict of interest.

References

1. von Boehmer, H., I. Aifantis, F. Gounari, O. Azogui, L. Haughn, I. Apostolou, E. Jaeckel, F. Grassi, and L. Klein. 2003. Thymic selection revisited: how essential is it? *Immunol. Rev.* 191: 62–78.
2. Anderson, M. S., E. S. Venanzi, Z. Chen, S. P. Berzins, C. Benoist, and D. Mathis. 2005. The cellular mechanism of Aire control of T cell tolerance. *Immunity* 23: 227–239.
3. Anderson, M. S., E. S. Venanzi, L. Klein, Z. Chen, S. P. Berzins, S. J. Turley, H. von Boehmer, R. Bronson, A. Dierich, C. Benoist, and D. Mathis. 2002. Projection of an immunological self shadow within the thymus by the aire protein. *Science* 298: 1395–1401.
4. Liston, A., S. Lesage, J. Wilson, L. Peltonen, and C. C. Goodnow. 2003. Aire regulates negative selection of organ-specific T cells. *Nat. Immunol.* 4: 350–354.
5. Anderson, G., K. M. Partington, and E. J. Jenkinson. 1998. Differential effects of peptide diversity and stromal cell type in positive and negative selection in the thymus. *J. Immunol.* 161: 6599–6603.
6. Marrack, P., D. Lo, R. Brinster, R. Palmiter, L. Burkly, R. H. Flavell, and J. Kappler. 1988. The effect of thymus environment on T cell development and tolerance. *Cell* 53: 627–634.
7. Matzinger, P., and S. Guerder. 1989. Does T-cell tolerance require a dedicated antigen-presenting cell? *Nature* 338: 74–76.
8. Wu, L., and K. Shortman. 2005. Heterogeneity of thymic dendritic cells. *Semin. Immunol.* 17: 304–312.
9. Liu, Y. J. 2006. A unified theory of central tolerance in the thymus. *Trends Immunol.* 27: 215–221.
10. Bendriss-Vermare, N., C. Barthelemy, I. Durand, C. Bruand, C. Dezutter-Dambuyant, N. Moulian, S. Berrih-Aknin, C. Caux, G. Trinchieri, and F. Briere. 2001. Human

thymus contains IFN-α-producing CD11c$^-$, myeloid CD11c$^+$, and mature interdigitating dendritic cells. *J. Clin. Invest.* 107: 835–844.
11. Sprent, J., and S. R. Webb. 1995. Intrathymic and extrathymic clonal deletion of T cells. *Curr. Opin. Immunol.* 7: 196–205.
12. Heino, M., P. Peterson, N. Sillanpaa, S. Guerin, L. Wu, G. Anderson, H. S. Scott, S. E. Antonarakis, J. Kudoh, N. Shimizu, et al. 2000. RNA and protein expression of the murine *autoimmune regulator gene (Aire)* in normal, RelB-deficient and in NOD mouse. *Eur. J. Immunol.* 30: 1884–1893.
13. Kyewski, B., and J. Derbinski. 2004. Self-representation in the thymus: an extended view. *Nat. Rev. Immunol.* 4: 688–698.
14. Proietto, A. I., S. van Dommelen, P. Zhou, A. Rizzitelli, A. D'Amico, R. J. Steptoe, S. H. Naik, M. H. Lahoud, Y. Liu, P. Zheng, et al. 2008. Dendritic cells in the thymus contribute to T-regulatory cell induction. *Proc. Natl. Acad. Sci. USA* 105: 19869–19874.
15. Heinzel, K., C. Benz, and C. C. Bleul. 2007. A silent chemokine receptor regulates steady-state leukocyte homing in vivo. *Proc. Natl. Acad. Sci. USA* 104: 8421–8426.
16. Kim, C. H. 2005. The greater chemotactic network for lymphocyte trafficking: chemokines and beyond. *Curr. Opin. Hematol.* 12: 298–304.
17. Schutyser, E., A. Richmond, and J. Van Damme. 2005. Involvement of CC chemokine ligand 18 (CCL18) in normal and pathological processes. *J. Leukocyte Biol.* 78: 14–26.
18. Vecchi, A., L. Massimiliano, S. Ramponi, W. Luini, S. Bernasconi, R. Bonecchi, P. Allavena, M. Parmentier, A. Mantovani, and S. Sozzani. 1999. Differential responsiveness to constitutive vs. inducible chemokines of immature and mature mouse dendritic cells. *J. Leukocyte Biol.* 66: 489–494.
19. Niess, J. H., S. Brand, X. Gu, L. Landsman, S. Jung, B. A. McCormick, J. M. Vyas, M. Boes, H. L. Ploegh, J. G. Fox, et al. 2005. CX3CR1-mediated dendritic cell access to the intestinal lumen and bacterial clearance. *Science* 307: 254–258.
20. Gao, J. L., T. A. Wynn, Y. Chang, E. J. Lee, H. E. Broxmeyer, S. Cooper, H. L. Tiffany, H. Westphal, J. Kwon-Chung, and P. M. Murphy. 1997. Impaired host defense, hematopoiesis, granulomatous inflammation and type 1-type 2 cytokine balance in mice lacking CC chemokine receptor 1. *J. Exp. Med.* 185: 1959–1968.
21. Combadiere, C., S. Potteaux, J. L. Gao, B. Esposito, S. Casanova, E. J. Lee, P. Debre, A. Tedgui, P. M. Murphy, and Z. Mallat. 2003. Decreased atherosclerotic lesion formation in CX3CR1/apolipoprotein E double knockout mice. *Circulation* 107: 1009–1016.
22. Murai, M., H. Yoneyama, T. Ezaki, M. Suematsu, Y. Terashima, A. Harada, H. Hamada, H. Asakura, H. Ishikawa, and K. Matsushima. 2003. Peyer's patch is the essential site in initiating murine acute and lethal graft-versus-host reaction. *Nat. Immunol.* 4: 154–160.
23. Kuziel, W. A., S. J. Morgan, T. C. Dawson, S. Griffin, O. Smithies, K. Ley, and N. Maeda. 1997. Severe reduction in leukocyte adhesion and monocyte extravasation in mice deficient in CC chemokine receptor 2. *Proc. Natl. Acad. Sci. USA* 94: 12053–12058.
24. Brewer, J. A., O. Kanagawa, B. P. Sleckman, and L. J. Muglia. 2002. Thymocyte apoptosis induced by T cell activation is mediated by glucocorticoids in vivo. *J. Immunol.* 169: 1837–1843.
25. Mayor, S., and R. E. Pagano. 2007. Pathways of clathrin-independent endocytosis. *Nat. Rev. Mol. Cell Biol.* 8: 603–612.
26. Sandvig, K., S. Olsnes, O. W. Petersen, and B. van Deurs. 1987. Acidification of the cytosol inhibits endocytosis from coated pits. *J. Cell Biol.* 105: 679–689.
27. Zal, T., A. Volkmann, and B. Stockinger. 1994. Mechanisms of tolerance induction in major histocompatibility complex class II-restricted T cells specific for a blood-borne self-antigen. *J. Exp. Med.* 180: 2089–2099.
28. Bubanovic, I. V. 2003. Failure of blood-thymus barrier as a mechanism of tumor and trophoblast escape. *Med. Hypotheses* 60: 315–320.
29. Balazs, M., F. Martin, T. Zhou, and J. Kearney. 2002. Blood dendritic cells interact with splenic marginal zone B cells to initiate T-independent immune responses. *Immunity* 17: 341–352.
30. Murphy, P. M., M. Baggiolini, I. F. Charo, C. A. Hebert, R. Horuk, K. Matsushima, L. H. Miller, J. J. Oppenheim, and C. A. Power. 2000. International union of pharmacology: XXII. Nomenclature for chemokine receptors. *Pharmacol. Rev.* 52: 145–176.
31. Vremec, D., J. Pooley, H. Hochrein, L. Wu, and K. Shortman. 2000. CD4 and CD8 expression by dendritic cell subtypes in mouse thymus and spleen. *J. Immunol.* 164: 2978–2986.
32. Ladi, E., T. A. Schwickert, T. Chtanova, Y. Chen, P. Herzmark, X. Yin, H. Aaron, S. W. Chan, M. Lipp, B. Roysam, and E. A. Robey. 2008. Thymocyte-dendritic cell interactions near sources of CCR7 ligands in the thymic cortex. *J. Immunol.* 181: 7014–7023.
33. McCaughtry, T. M., T. A. Baldwin, M. S. Wilken, and K. A. Hogquist. 2008. Clonal deletion of thymocytes can occur in the cortex with no involvement of the medulla. *J. Exp. Med.* 205: 2575–2584.
34. Sawanobori, Y., S. Ueha, M. Kurachi, T. Shimaoka, J. E. Talmadge, J. Abe, Y. Shono, M. Kitabatake, K. Kakimi, N. Mukaida, and K. Matsushima. 2008. Chemokine-mediated rapid turnover of myeloid-derived suppressor cells in tumor-bearing mice. *Blood* 111: 5457–5466.
35. Tsou, C. L., W. Peters, Y. Si, S. Slaymaker, A. M. Aslanian, S. P. Weisberg, M. Mack, and I. F. Charo. 2007. Critical roles for CCR2 and MCP-3 in monocyte mobilization from bone marrow and recruitment to inflammatory sites. *J. Clin. Invest.* 117: 902–909.
36. Mori, K., M. Itoi, N. Tsukamoto, H. Kubo, and T. Amagai. 2007. The perivascular space as a path of hematopoietic progenitor cells and mature T cells between the blood circulation and the thymic parenchyma. *Int. Immunol.* 19: 745–753.
37. Haribhai, D., D. Engle, M. Meyer, D. Donermeyer, J. M. White, and C. B. Williams. 2003. A threshold for central T cell tolerance to an inducible serum protein. *J. Immunol.* 170: 3007–3014.
38. Quinones, M. P., S. K. Ahuja, F. Jimenez, J. Schaefer, E. Garavito, A. Rao, G. Chenaux, R. L. Reddick, W. A. Kuziel, and S. S. Ahuja. 2004. Experimental arthritis in CC chemokine receptor 2-null mice closely mimics severe human rheumatoid arthritis. *J. Clin. Invest.* 113: 856–866.
39. Lauritzsen, G. F., P. O. Hofgaard, K. Schenck, and B. Bogen. 1998. Clonal deletion of thymocytes as a tumor escape mechanism. *Int. J. Cancer* 78: 216–222.
40. Paessens, L. C., D. M. Fluitsma, and Y. van Kooyk. 2008. Haematopoietic antigen-presenting cells in the human thymic cortex: evidence for a role in selection and removal of apoptotic thymocytes. *J. Pathol.* 214: 96–103.

Hepatology Research 2008; 38: 354–361 doi: 10.1111/j.1872-034X.2007.00284.x

Original Article

Intrahepatic status of regulatory T cells in autoimmune liver diseases and chronic viral hepatitis

Masashi Sakaki,[1] Kazumasa Hiroishi,[1] Toshiyuki Baba,[1] Takayoshi Ito,[1] Yuichi Hirayama,[1] Koji Saito,[2] Takahiko Tonoike,[3] Miki Kushima[3] and Michio Imawari[1]

[1]*Second Department of Internal Medicine,* [2]*First Department of Pathology and* [3]*Division of Hospital Pathology, Showa University School of Medicine, Tokyo, Japan*

Aim: Regulatory T cells (Tregs) maintain immunological tolerance and suppress autoreactive immune responses. We evaluated the intrahepatic status of Tregs in patients with autoimmune hepatitis (AIH), primary biliary cirrhosis (PBC), chronic hepatitis C (CH-C), or chronic hepatitis B (CH-B).

Methods: We analyzed 85 patients (20 AIH, 22 PBC, 27 CH-C, and 16 CH-B) and 14 controls. Using liver tissue samples obtained by needle biopsy or from marginal parts of resected metastatic liver tumors in the controls, immunohistochemical analyses of forkhead box $P3^+$, which is a specific marker for Tregs, $CD4^+$, and $CD8^+$ cells were performed.

Results: Intrahepatic Tregs were significantly more infiltrated in patients with liver diseases than in the controls. There were significantly fewer intrahepatic Tregs in the AIH patients than in the PBC patients ($P = 0.037$). Patients with a low frequency of intrahepatic Tregs were detected significantly more in the AIH and CH-B groups than in the PBC and CH-C groups ($P < 0.05$). In addition, the frequency of Tregs decreased in the liver of PBC patients as the pathological stage of the disease advanced. We found significantly less infiltration of $CD4^+$ T cells in AIH than in other diseases ($P < 0.05$). Liver-infiltrating $CD8^+$ T cells were detected more frequently in the CH-B group than in other groups ($P < 0.003$).

Conclusion: Intrahepatic Tregs were increased in both patients with autoimmune liver diseases and those with viral hepatitis. In autoimmune liver diseases, intrahepatic Tregs were fewer in the AIH patients than in the PBC patients.

Key words: autoimmune hepatitis, chronic hepatitis, forkhead box P3, primary biliary cirrhosis, regulatory T cells

INTRODUCTION

T-CELL RESPONSES are implicated in host immune defense against microbes as well as immunopathogenesis of certain diseases, such as viral hepatitis. An appropriate T-cell response leads to the eradication of microbes, while a weak response may result in persistent infection. If the T-cell activation is too potent, however, severe inflammation or autoimmune disease may develop. The detailed mechanisms that lead to the breakdown of self-tolerance and the subsequent development of autoimmune disease are still unknown; however, the mechanisms are likely to involve the failure of homeostatic processes that keep the response against self-antigens under control.[1]

T-cell populations regulate and control the balance of immune responses. The $CD4^+$ and $CD25^+$ regulatory T cells (Tregs) are crucial for maintaining immunologic self-tolerance and negative control of various immune responses. The majority of Tregs are produced by the thymus as a functionally distinct T-cell subpopulation and are responsible for maintaining peripheral tolerance. Genetic abnormalities in the development and function of this Treg population can cause autoimmune disease, immunopathology, and allergy in humans.[2] In addition, there are different T-cell subpopulations with regulatory functions, such as natural killer T cells, T helper 3, T regulatory 1, $CD8^+$ and $CD28^-$, and $\gamma\delta$ T cells. These types of T cells may also prevent the activation of autoreactive T cells and be involved in the failure of homeostasis.[1]

Although several cell-surface molecules, such as CD25, glucocorticoid-induced tumor necrosis factor

Correspondence: Professor Michio Imawari, Second Department of Internal Medicine, Showa University School of Medicine, 1-5-8 Hatanodai, Shinagawa-ku, Tokyo 142-8666, Japan. Email: imawari@med.showa-u.ac.jp
Received 14 June 2007; revision 8 September 2007; accepted 9 September 2007.

receptor family-related gene/protein, and cytotoxic T lymphocyte-associated molecule-4, have been reported as Treg markers, these molecules are also expressed on activated T cells derived from $CD4^+$ and $CD25^-$ naïve T cells.[3] Transcription factor forkhead box P3 (FOXP3) is expressed in $CD4^+$ and $CD25^+$ Tregs as a master control molecule for their development and function in mice and humans, thus, FOXP3 is thought to be a specific marker of Tregs.

Autoimmune mechanisms are involved in autoimmune hepatitis (AIH) and primary biliary cirrhosis (PBC). AIH is an inflammatory liver disease characterized by high levels of transaminases, circulating autoantibodies, hyper-γ-globulinemia, histological evidence of interface hepatitis, and response to immunosuppressive treatment.[4,5] PBC is an enigmatic liver disease characterized by the chronic non-suppurative destruction of small intrahepatic bile ducts, portal inflammation, and the presence of antimitochondrial antibodies (AMA).[6,7] The presence of AMA and autoreactive T and B cells, in conjunction with the co-occurrence of other autoimmune diseases, characterizes PBC as a typical autoimmune disease.[8] Although the etiology of PBC remains obscure, recent data suggest that autoreactive T-cell responses play a major role in its pathophysiology.[9–12]

Hepatitis C virus (HCV) infection is often asymptomatic, and approximately 80% of infected patients progress to chronic hepatitis.[13] After HCV infection, interaction between the innate and adaptive immune responses plays a pivotal role in perpetuation or clearance of HCV infection. T helper 1-type (Th1) cytokines, such as interferon (IFN)-γ and interleukin (IL)-2, are involved in cell-mediated immunity and play a crucial role in protection against intracellular pathogens.[14] A weak cellular immune response is thought to be one of the mechanisms of HCV persistence.

In hepatitis B virus (HBV) infection, a multispecific $CD4^+$ and $CD8^+$ T cell with a Th1 cytokine profile is also important for control of the infection.[15] These multispecific T-cell responses are maintained for decades after clinical recovery. However, these responses are lacking in patients with chronic HBV infection, and the mechanism of T-cell hyporesponsiveness or tolerance is still unknown.

The frequency of Tregs in the peripheral blood was decreased in patients with AIH and PBC and increased in patients with chronic hepatitis C (CH-C) and chronic hepatitis B (CH-B) compared with the healthy controls.[16] However, there are few reports investigating the intrahepatic status of Tregs. In the present study, we analyzed and compared the intrahepatic status of Tregs in patients with AIH, PBC, CH-C, and CH-B because liver-infiltrating immune cells should reflect the status of disease and pathogenesis more directly than peripheral cells.

METHODS

Patients and liver tissue

NEEDLE BIOPSIES WERE performed to obtain liver tissue from 85 patients, consisting of 20 AIH patients, 22 PBC patients, 27 CH-C patients, and 16 CH-B patients. All patients had a persistently increased level of serum alanine aminotransferase (ALT; >30 IU/L). The diagnosis of each case was based on reliable clinical and laboratory data and was independently confirmed histologically by two pathologists who specialize in liver diseases. All AIH patients were antinuclear antibody positive or antismooth muscle antibody positive, and all had histological features of interface hepatitis. Patients with morbid changes in bile duct were excluded individually by retrograde radiological cholangiography or magnetic resonance cholangiopancreatography. Patients with overlap syndrome were also excluded from this study. All PBC patients were AMA positive and fulfilled the diagnostic criteria of PBC based on internationally accepted standards. Livers from PBC patients were staged histologically by Scheuer's classification. Seventeen and five patients were of stage 1 and of stages 2/3/4, respectively. We included 14 patients with metastatic liver tumors as the controls. The control patients were not infected with HBV (negative for hepatitis B surface antigen) or HCV (negative for anti-HCV antibody), and they had no history of autoimmune diseases and were negative for autoimmune antibodies. Liver tissue from control patients was obtained from a marginal part of the resected liver in which the histological examination was normal. Table 1 shows the patients' characteristics. All patients gave written informed consent according to a protocol approved by the Ethical Committee of Showa University.

Immunohistochemical staining

Liver needle biopsies and resected tissues were obtained from the 99 patients, as described earlier. All tissues were fixed in 10% neutral-buffered formalin and embedded in paraffin, and 3 μm-thick serial sections were cut from each paraffin block. Each specimen contained at least three portal tracts encompassing interlobular bile ducts, and a total of 297 portal tracts were counted. Antigen retrieval for CD4 and FOXP3 staining

Table 1 Characteristics of the patients and controls analyzed in this study

Group (number)	AIH (20)	PBC (22)	CH-C (27)	CH-B (16)	Control (14)
Female (%)	95.0*,†,††	90.9†,‡‡,¶	40.7	18.8	28.6
Age (years)	55.8 ± 13.8†	55.5 ± 11.2‡‡	49.8 ± 11.9§,§§	38.1 ± 11.6$^{\|}$	59.1 ± 14.2
ALT (IU/L)	393 ± 462*,**,††	113 ± 139‡‡,¶	85 ± 57§,§§	295 ± 351$^{\|}$	17 ± 9
AST (IU/L)	306 ± 393*,**,††	88 ± 78¶	60 ± 40§,§§	148 ± 141$^{\|}$	22 ± 9
ALP (IU/L)	495 ± 300*,**,†	842 ± 547†,‡‡,¶	268 ± 85	320 ± 96	316 ± 171
IgG (mg/dL)	2639 ± 1163*,**	1837 ± 584	1794 ± 290	n.d.	n.d.
IgM (mg/dL)	334 ± 355**	466 ± 231‡	129 ± 67	n.d.	n.d.

Significance was assessed with Fisher's exact probability test. $P < 0.05$ (*AIH versus PBC, **AIH versus CH-C, †AIH versus CH-B, ††AIH versus Control, ‡PBC versus CH-C, ‡‡PBC versus CH-B, ¶PBC versus Control, §CH-C versus CH-B, §§CH-C versus Control, $^{\|}$CH-B versus Control). Values are mean ± standard deviation. AIH, autoimmune hepatitis; ALP, alkaline phosphatase; ALT, alanine aminotransferase; AST, aspartate aminotransferase; CH-B, chronic hepatitis B; CH-C, chronic hepatitis C; IgG, immunoglobulin G; IgM, immunoglobulin M; n.a., not determined; PBC, primary biliary cirrhosis.

was achieved by pressure cooking for 5 min in citrate buffer (pH 7.0), while antigen retrieval for CD8 staining was achieved by microwaving for 15 min in citrate buffer (pH 7.0). For CD4 or CD8 immunohistochemical staining, anti-CD4 monoclonal antibody (mAb; Nichirei Biosciences, Tokyo, Japan) or anti-CD8 mAb (Dako Cytomation, Tokyo, Japan) and biotinylated goat antimouse immunoglobulin G (IgG; Dako ChemMate Envision kit/HRP[DAB], Dako, Japan) were used. FOXP3 expression was analyzed by immunostaining with a goat antihuman FOXP3 polyclonal antibody (ab22510; Abcam, Cambridge, UK) and biotinylated rabbit antigoat IgG (Dako ChemMate Envision kit/HRP[DAB]). The slides were stained with hematoxylin following immunohistochemical staining.

Evaluation of frequency of FOXP3-, CD4-, and CD8-positive cells

To evaluate and compare the distribution and frequency of cells positive for FOXP3, CD4, and CD8, three small- to medium-sized portal tract areas were selected for investigation with an optical microscope. The same visual fields were chosen and examined using serial sections. The numbers of FOXP3-, CD4-, or CD8-positive cells contained within the three portal tract areas from each specimen were counted at a magnification of ×400 by two independent observers in a blinded fashion. To correct for differences in the sizes of the portal tracts, the proportion of FOXP3^{+} Tregs was determined as follows: %FOXP3 = (counts of FOXP3^{+} Tregs/counts of total mononuclear cells) × 100, which is a total mononuclear cell-corrected value for FOXP3^{+} CD4^{+} and CD8^{+} T cells in total mononuclear cells were also calculated.

Statistical analyses

Significance was assessed with the Mann–Whitney *U*-test or Fisher's exact probability test. Differences between groups were considered statistically significant when the *P*-value was less than 0.05.

RESULTS

Intrahepatic Tregs were significantly more infiltrated in patients with liver diseases than in the controls

TO COMPARE THE frequencies of intrahepatic FOXP3^{+} Tregs between the liver diseases, we determined the percentage of FOXP3, as described in Methods. As shown in Figure 1, the frequency of FOXP3^{+} T cells in patients with AIH, PBC, CH-C, or CH-B was significantly much higher than that in the control patients. Interestingly, there were significantly fewer FOXP3^{+} T cells in the liver tissues of AIH patients than in those of PBC patients ($P = 0.037$). The frequency of intrahepatic FOXP3^{+} Tregs in the AIH patients was not different from that in the patients with CH-C or CH-B.

Patients with a low frequency of intrahepatic Tregs were detected significantly more in the AIH and CH-B groups than in the PBC and CH-C groups

Since the patients with numerous intrahepatic FOXP3^{+} Tregs were observed in the PBC and CH-C groups, we separated the patients into two groups according to the frequency of intrahepatic Tregs. The patients were divided into those with FOXP3^{+} cells of less than 9% and those with FOXP3^{+} cells of 9% or more: this level

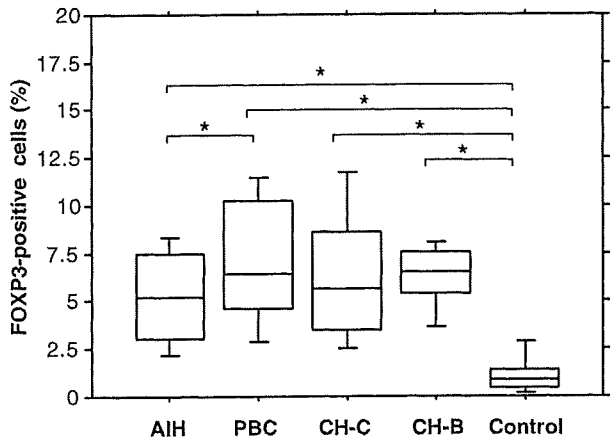

Figure 1 Intrahepatic forkhead box P3⁺ (FOXP3⁺) T cells in autoimmune hepatitis (AIH), primary biliary cirrhosis (PBC), chronic hepatitis C (CH-C), chronic hepatitis B (CH-B), and controls. To compare intrahepatic FOXP3⁺ cell status, intrahepatic FOXP3⁺ cells in patients with AIH, PBC, CH-C, and CH-B were stained. For the enumeration of positive mononuclear cells, mononuclear cells were counted in three high-powered fields (×400) by two independent observers in a blinded fashion. For each sample, the mean percentage of positive cells was chosen. Results are expressed as the median and range of all tested patents in each group. $P < 0.05$.

was decided arbitrarily as follows: (mean percentage of FOXP3 of controls + 3 standard deviation) × 2. When the number of patients with a high frequency of intrahepatic Tregs (%FOXP3 ≥9%) and that with a low frequency (%FOXP3 <9%) were compared for each liver disease, patients who had a low frequency of intrahepatic Tregs were detected significantly more in the AIH group than in PBC and CH-C groups as shown in Table 2. In addition, more patients with low frequency Treg infiltration were found in the CH-B group than in the PBC and CH-C groups. Thus, PBC is characterized by higher frequency of FOXP3⁺ cells compared to AIH, whereas the number and profiles of liver-infiltrating T cells are comparable. In viral hepatitis, a higher frequency of FOXP3⁺ cells is observed in CH-C, while higher frequency of CD4⁺ or CD8⁺ cells is characteristic for HBV-infected liver.

Table 3 Comparison of the intrahepatic Tregs frequency with histological stages in PBC patients

	<9%	≥9%	Total
Early stage	8	9	17
Advanced stage	5	0	5
Total	13	9	22

$P = 0.034$. PBC patients were divided into two groups as early stage (Scheuer's classification stage 1) and advanced stage (stages 2/3/4). Number of patients with a high frequency of intrahepatic regulatory T cells (Tregs; %FOXP3 ≥9%) and that with a low frequency (%FOXP3 <9%) were compared for each stage. PBC, primary biliary cirrhosis.

When the PBC patients were divided into two groups as early stage (Scheuer's classification stage 1) and advanced stage (stages 2/3/4), the frequency of Tregs was higher than 9% in nine of 17 (53%) PBC patients with early histological stage, while that of Tregs was below 9% in all patients with advanced stage ($P = 0.034$), as shown in Table 3. Furthermore, as shown in Figure 2, more FOXP3⁺ T-cell infiltration was seen in the early stage than in the advanced stage (8.03 ± 3.50 *vs* 4.47 ± 1.40, $P = 0.041$). Therefore, it was thought that the frequency of Tregs decreased in the liver of PBC patients as the pathological stage of the disease advanced.

Frequency of intrahepatic CD4⁺ T cells was lower in AIH patients, while the frequency of intrahepatic CD8⁺ T cells was higher in CH-B patients

We evaluated the intrahepatic frequencies of CD4⁺ cells as well as CD8⁺ cells to investigate whether these

Table 2 Comparison of the number of patients with high frequency of intrahepatic Tregs with those with low frequency

	<9%	≥9%	Versus PBC*	Versus CH-C**
AIH ($n = 20$)	20	0	$P = 0.001$	$P = 0.014$
PBC ($n = 22$)	13	9	-	$P = 0.266$
CH-C ($n = 27$)	20	7	$P = 0.266$	-
CH-B ($n = 16$)	16	0	$P = 0.003$	$P = 0.026$
Control ($n = 14$)	14	0	$P = 0.006$	$P = 0.036$

Significance was assessed with Fisher's exact probability test. *P*-values are shown as VS PBC group(*) and VS CH-C(**) group.
AIH, autoimmune hepatitis; CH-B, chronic hepatitis B; CH-C, chronic hepatitis C; PBC, primary biliary cirrhosis; Tregs, regulatory T cells